Dual function of VGLL4 in muscle regeneration

Xue Feng[1,†], Zuoyun Wang[1,†], Fei Wang[1,†], Tiantian Lu[1], Jinjin Xu[1], Xueyan Ma[1], Jinhui Li[1], Lingli He[1] (ID), Wenxiang Zhang[1], Sheng Li[1], Wenjun Yang[1], Shu Zhang[1], Gaoxiang Ge[1], Yun Zhao[1,2] (ID), Ping Hu[1,3,*] (ID) & Lei Zhang[1,2,**] (ID)

Abstract

VGLL4 has previously been identified as a negative regulator of YAP. Here we show that VGLL4 regulates muscle regeneration in both YAP-dependent and YAP-independent manners at different stages. Knockout of VGLL4 in mice leads to smaller myofiber size and defective muscle contraction force. Furthermore, our studies reveal that knockout of VGLL4 results in increased muscle satellite cells proliferation and impaired myoblast differentiation, which ultimately leads to delayed muscle regeneration. Mechanistically, the results show that VGLL4 works as a conventional repressor of YAP at the proliferation stage of muscle regeneration. At the differentiation stage, VGLL4 acts as a co-activator of TEAD4 to promote MyoG transactivation and facilitate the initiation of differentiation in a YAP-independent manner. Moreover, VGLL4 stabilizes the protein–protein interactions between MyoD and TEAD4 to achieve efficient MyoG transactivation. Our findings define the dual roles of VGLL4 in regulating muscle regeneration at different stages and may open novel therapeutic perspectives for muscle regeneration.

Introduction

Skeletal muscle has regeneration ability due to the existence of muscle satellite cells (MuSCs; Murphy et al, 2011). MuSCs are resident adult stem cells that are activated after muscle injury and have the differentiation ability to form myotubes (Brack & Rando, 2012). The proliferation and differentiation of MuSCs are regulated through the activation of multiple signaling pathways. Skeletal muscle development and postnatal muscle regeneration are tightly regulated by

muscle-specific transcriptional factors. Several basic helix-loop-helix (bHLH) transcription family members, known as myogenic regulatory factors (MRFs), play critical regulatory roles in myogenesis (Buckingham & Rigby, 2014). MyoD is one of the MRFs and considered to be the master regulator of myogenesis (Berkes & Tapscott, 2005), which could transdifferentiate non-muscle cells to muscle cells (Weintraub et al, 1991). MyoD forms a heterodimer with E12 or E47 that recognizes and binds to the E-box elements (Blackwell & Weintraub, 1990; Shirakata & Paterson, 1995). In addition, other bHLH transcription factors such as Myf5, MRF4, and Myogenin (MyoG) are also MRFs (Buckingham & Rigby, 2014). MyoD directly activates the transcription of MyoG via binding to MyoG's E-box promoter region, which further activates the transcription of genes required for myoblast terminal differentiation such as MyHC and MCK (Yun & Wold, 1996; Tapscott, 2005).

Hippo pathway, evolutionarily conserved from *Drosophila* to mammals, controls organ size and tissue homeostasis (Zhao et al, 2011). Hippo pathway is comprised of a core kinase cascade that consists of MST1/2, LATS1/2, SAV1, and MOB1 (Pan, 2010). Phosphorylation of transcription co-activators YAP and TAZ by the kinase cascade retains them in the cytoplasm, leading to inactivation of the Hippo downstream transcription factors TEADs (TEAD1-4; Dong et al, 2007; Zhao et al, 2007). Several target genes of YAP-TEADs have been identified, such as cell cycle and cell survival regulators CTGF and CYR61 (Zhang et al, 2008; Zhao et al, 2008; Pobbati & Hong, 2013). Disruption of Hippo pathway leads to tumorigenesis and dysregulation of organ size (Harvey et al, 2013; Yu et al, 2015). Hippo pathway has also been implicated in promoting stem cells self-renewal and tissue repair (Zhao et al, 2011). Several critical Hippo downstream factors have been suggested to play regulatory roles in skeletal muscle development and muscle regeneration (Judson et al, 2012; Joshi et al, 2017); however, the regulatory mechanism remains poorly defined.

VGLL4 is a member of the vestigial-like (VGLL) family transcription co-factors (VGLL1-4) that contain Tondu (TDU) domains (Chen et al, 2004). VGLL1-4 do not contain DNA-binding domain, and they exert their transcriptional regulatory functions mainly through interaction with members of TEAD transcription factor family via their

TDU domains (Maeda *et al*, 2002; Chen *et al*, 2004). In *Drosophila*, Tgi/SdBP, an ortholog of VGLL4, is discovered from genetic screens for Yki-Sd (YAP-TEADs) antagonists (Guo *et al*, 2013; Koontz *et al*, 2013). In mammals, VGLL4 similarly competes with YAP for TEADs binding and represses the pro-proliferative and oncogenic activities of YAP (Jiao *et al*, 2014; Zhang *et al*, 2014). Recently, we reported that conditional knockout of VGLL4 in endothelial cells results in enhanced cell proliferation, which ultimately leads to heart valve thickening and valve malformation (Yu *et al*, 2019). However, the role of VGLL4 in skeletal muscle regeneration especially in muscle differentiation remains to be investigated.

Here we uncover the dual function and the underlying mechanisms of VGLL4 in governing muscle regeneration. Our *in vitro* and *in vivo* studies demonstrated that knockout of VGLL4 enhanced MuSCs proliferation via antagonizing with YAP. Knockout of YAP in MuSCs constrained the hyper proliferation of MuSCs induced by VGLL4 deletion. We further identified that conditional knockout of VGLL4 in MuSCs resulted in impaired muscle differentiation. Mechanistically, TEAD4 directly regulated MyoG transcription by binding to the TEAD binding site in MyoG promoter. VGLL4 acted as an indispensible co-activator of TEAD4 for MyoG transactivation and muscle differentiation. Furthermore, VGLL4 enhanced the binding between TEAD4 and MyoD to achieve efficient MyoG transactivation. Our studies identified VGLL4 as a novel activator in regulating muscle regeneration at the differentiation stage, which provides new insights into the YAP-independent role of VGLL4 in skeletal muscle regeneration.

Results

VGLL4 null mice display reduced myofiber size and functional defects in skeletal muscle

VGLL4 is a transcriptional suppressor that inhibits YAP-induced overgrowth and tumorigenesis (Jiao *et al*, 2014). In order to investigate the function of VGLL4 in skeletal muscle, we analyzed the constitutive VGLL4 knockout mice generated by our laboratory (Fig EV1A and B; Yu *et al*, 2019). Expression of VGLL4 was abolished in muscle tissues of VGLL4 knockout ($Vgll4^{-/-}$) mice (Fig EV1C and D). The body size was significantly smaller, and the body mass was decreased in VGLL4 null mice compared with their wild-type ($Vgll4^{+/+}$) littermates (Figs 1A and EV1E). The sizes of tibialis anterior (TA) and extensor digitorum longus (EDL) muscles were also smaller in $Vgll4^{-/-}$ mice (Fig 1B), as indicated by decreased percentages of both TA and EDL muscle weight to the whole body weight (Fig 1C and D). However, the ratios of kidney weight and spleen weight to the whole body weight showed no obvious changes (Fig EV1F and G), suggesting there is a relatively specific reduction of skeletal muscle in VGLL4 knockout mice. Furthermore, the ratios of both TA and EDL muscles weight to the tibia length were also reduced (Fig EV1H and I). We next examined whether the smaller muscle in $Vgll4^{-/-}$ mice is due to the reduction of fiber number or fiber size. The fiber number in TA muscle's maximum cross-sectional area showed no change (Fig 1E); however, the fiber size was significantly smaller in $Vgll4^{-/-}$ mice compared to that in the $Vgll4^{+/+}$ littermates (Figs 1F and G, and EV1J), suggesting that the smaller muscle size is due to the reduction of the

myofiber size. Moreover, the EDL muscles were significantly smaller and displayed disorganized fibers in VGLL4 knockout mice under scanning electronic microscopy (SEM; Fig EV1K). The diameter of isolated single fibers from EDL muscles was decreased in $Vgll4^{-/-}$ mice as well (Fig 1H and I). In order to determine whether the smaller fiber size leads to any functional defects, tetanus and twitch tensions were measured. Consistent with the reduced myofiber size, $Vgll4^{-/-}$ mice showed significantly lower contraction forces in their TA muscles (Fig 1J and K). Distance of running exhaustion measured by treadmill test was significantly shorter in $Vgll4^{-/-}$ mice compared with control mice (Fig 1L). Taken together, these results demonstrate that VGLL4 plays essential roles in regulating skeletal muscle size and muscle function.

VGLL4 is essential for maintaining the function and homeostasis of MuSCs

The smaller myofiber size may be due to abnormal functions of embryonic myoblasts or postnatal MuSCs defects. To examine whether the reduced muscle size in $Vgll4^{-/-}$ mice is caused by impaired embryonic myoblasts activity, we first performed HE staining of postnatal (P0) muscles from neonatal $Vgll4^{+/+}$ and $Vgll4^{-/-}$ mice. Notably, there was no obvious difference in muscle fiber formation of $Vgll4^{-/-}$ pups compared with control littermates (Fig EV2A and B), indicating normal embryonic myoblasts activity. Given that the MuSCs, a population of postnatal muscle stem cells, represent a distinct lineage of myogenic progenitors responsible for the postnatal growth (Seale & Rudnicki, 2000), we further isolated MuSCs from adult $Vgll4^{+/+}$ and $Vgll4^{-/-}$ mice and checked the effects of VGLL4 on MuSCs (Fig EV2C). Our data showed that $Vgll4^{-/-}$ MuSCs proliferated faster than their wild-type counterpart (Fig 2A). On the contrary, the differentiation process was impaired in VGLL4 knockout MuSCs, as indicated by lower fusion index and shorter myotubes formation (Figs 2B and C, and EV2D). MyoG, the key transcription factor of myoblast differentiation, can further activate the expression levels of the terminal differentiation markers MyHC and MCK (Hasty *et al*, 1993; Nabeshima *et al*, 1993; Yun & Wold, 1996; Allen *et al*, 2001). Consistent with the morphological difference, we found that the expression levels of MyoG, MyHC, and MCK were lower in $Vgll4^{-/-}$ myotubes (Figs 2D–F and EV2E). These results suggest that VGLL4 restrains MuSCs proliferation but promotes MuSCs differentiation.

To further confirm that the muscle defects are due to defective MuSCs homeostasis, we generated MuSCs-specific VGLL4 knockout mice ($Pax7$-$Cre^{ERT2/ERT2}$,$Vgll4^{f/f}$) by crossing $Pax7$-$Cre^{ERT2/ERT2}$ mice with $Vgll4^{f/f}$ mice. VGLL4 was depleted in MuSCs by administration of tamoxifen (TAM) to $Pax7$-$Cre^{ERT2/ERT2}$,$Vgll4^{f/f}$ mice at postnatal day 5 (P5; Figs 2G and EV2F and G). Both the body size and skeletal muscle size were dramatically smaller in MuSCs-specific VGLL4 knockout ($Vgll4^{CKO}$) mice (Fig 2H and I). The ratios of both TA and EDL muscles weight to the body weight were obviously lower in $Vgll4^{CKO}$ mice (Fig 2J and K). The percentages of both TA and EDL muscles weight to the tibia length were also decreased in $Vgll4^{CKO}$ mice (Fig EV2H and I). Furthermore, significant reduction of the myofiber size was observed in $Vgll4^{CKO}$ mice (Fig 2L and M). These data demonstrate that VGLL4 plays an important role in maintaining the function and homeostasis of MuSCs.
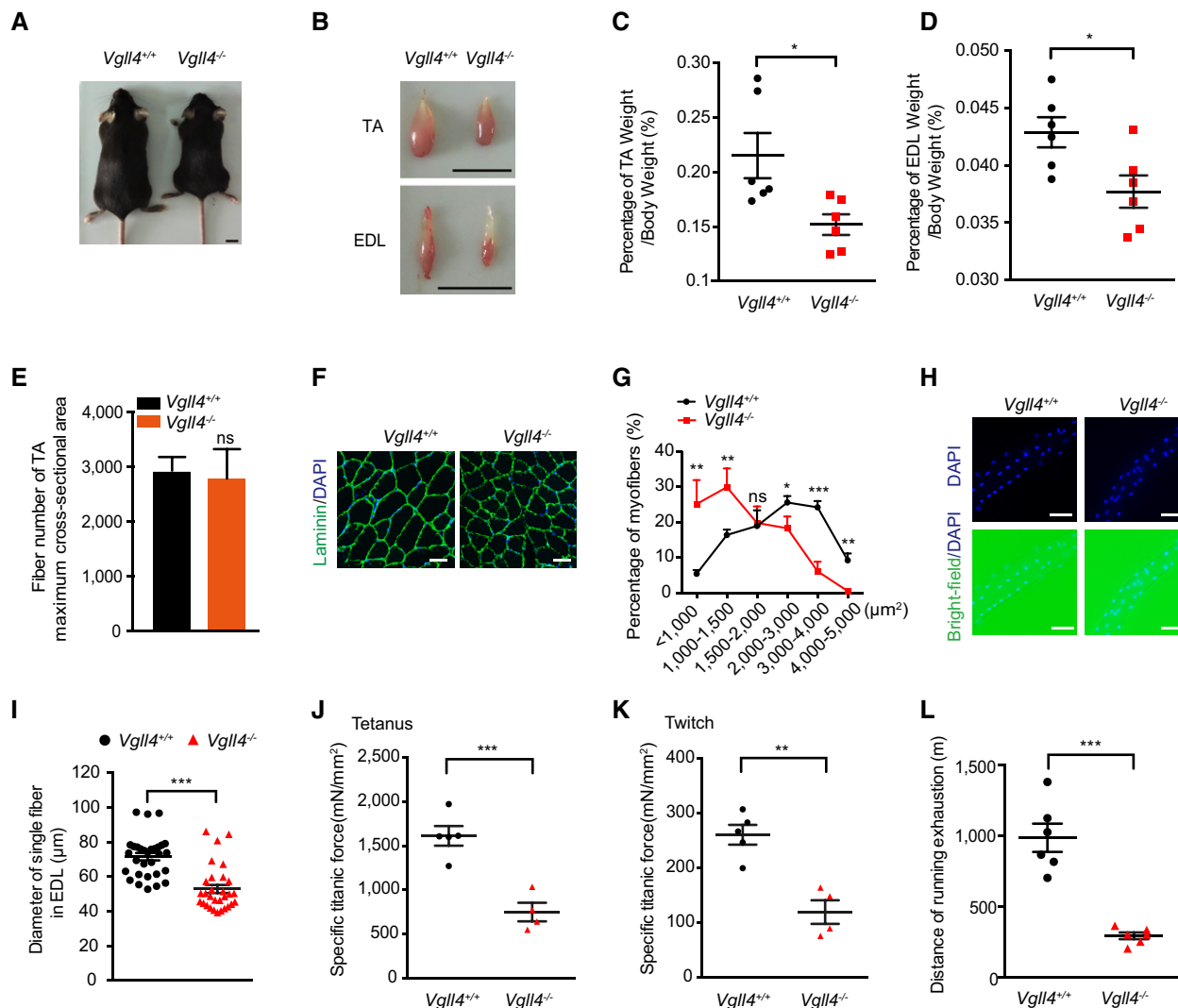
Figure 1. VGLL4 knockout leads to smaller myofiber size and functional defects in skeletal muscle.

A Representative photographs of Vgll4+/+ and Vgll4−/− littermates at 12 weeks of age. Scale bars: 1 cm.
B Representative photographs of the TA and EDL muscles from Vgll4+/+ and Vgll4−/− littermates at 12 weeks of age. Scale bars: 1 cm.
C Ratio analysis of TA muscle weight to the whole body weight from Vgll4+/+ and Vgll4−/− mice at 12 weeks of age (n = 6 mice).
D Ratio analysis of EDL muscle weight to the whole body weight from Vgll4+/+ and Vgll4−/− mice at 12 weeks of age (n = 6 mice).
E Statistical analysis of fiber number from TA muscles' maximum cross-sectional area in Vgll4+/+ and Vgll4−/− mice at 12 weeks of age (n = 4 mice).
F Representative immunostaining for Laminin (green) and DAPI (blue) of TA muscles' maximum cross-sections from Vgll4+/+ and Vgll4−/− mice at 12 weeks of age. Scale bars: 50 μm.
G Percentage distribution of myofibers in TA muscles' maximum cross-sectional area derived from Vgll4+/+ and Vgll4−/− mice at 12 weeks of age (n = 4 mice).
H Representative immunostaining for DAPI (blue) of EDL muscles isolated from Vgll4+/+ and Vgll4−/− mice at 12 weeks of age. The merged images of DAPI and bright-field were also shown. Scale bars: 50 μm.
I Quantification of the diameter of single fiber measured from Vgll4+/+ and Vgll4−/− mice's EDL muscles (n = 30 single fibers isolated from 5 mice per group).
J A recording of fused tetanic contraction was measured in situ in TA muscles from Vgll4+/+ and Vgll4−/− mice at 12 weeks of age. Vgll4+/+: n = 5 mice, Vgll4−/−: n = 4 mice.
K A single max twitch force was measured in situ in TA muscles from Vgll4+/+ and Vgll4−/− mice at 12 weeks of age. Vgll4+/+: n = 5 mice, Vgll4−/−: n = 4 mice.
L Distances of running exhustion were measured from Vgll4+/+ and Vgll4−/− mice at 12 weeks of age. n = 6 mice.

Data information: In (C, D, E, G, I, J, K, L), data were presented as mean ± SEM; *P < 0.05, **P < 0.01, ***P < 0.001, ns: no significance; unpaired Student t-test.

VGLL4 is transient increased in response to muscle injury and its ablation enhances MuSCs proliferation during muscle regeneration

MuSCs are the major force that drives postnatal muscle repair (Murphy *et al*, 2011). We next investigated whether VGLL4 is required for muscle regeneration. We noticed that VGLL4 expression was robustly induced at day 1 and peaked at day 3 after muscle injury at both mRNA and protein levels (Fig 3A and B). We further identified that VGLL4 mainly localized in the nucleus and its expression was dramatically increased after muscle injury in the transgenic Vgll4eGFP/eGFP reporter mice (Fig 3C), in which
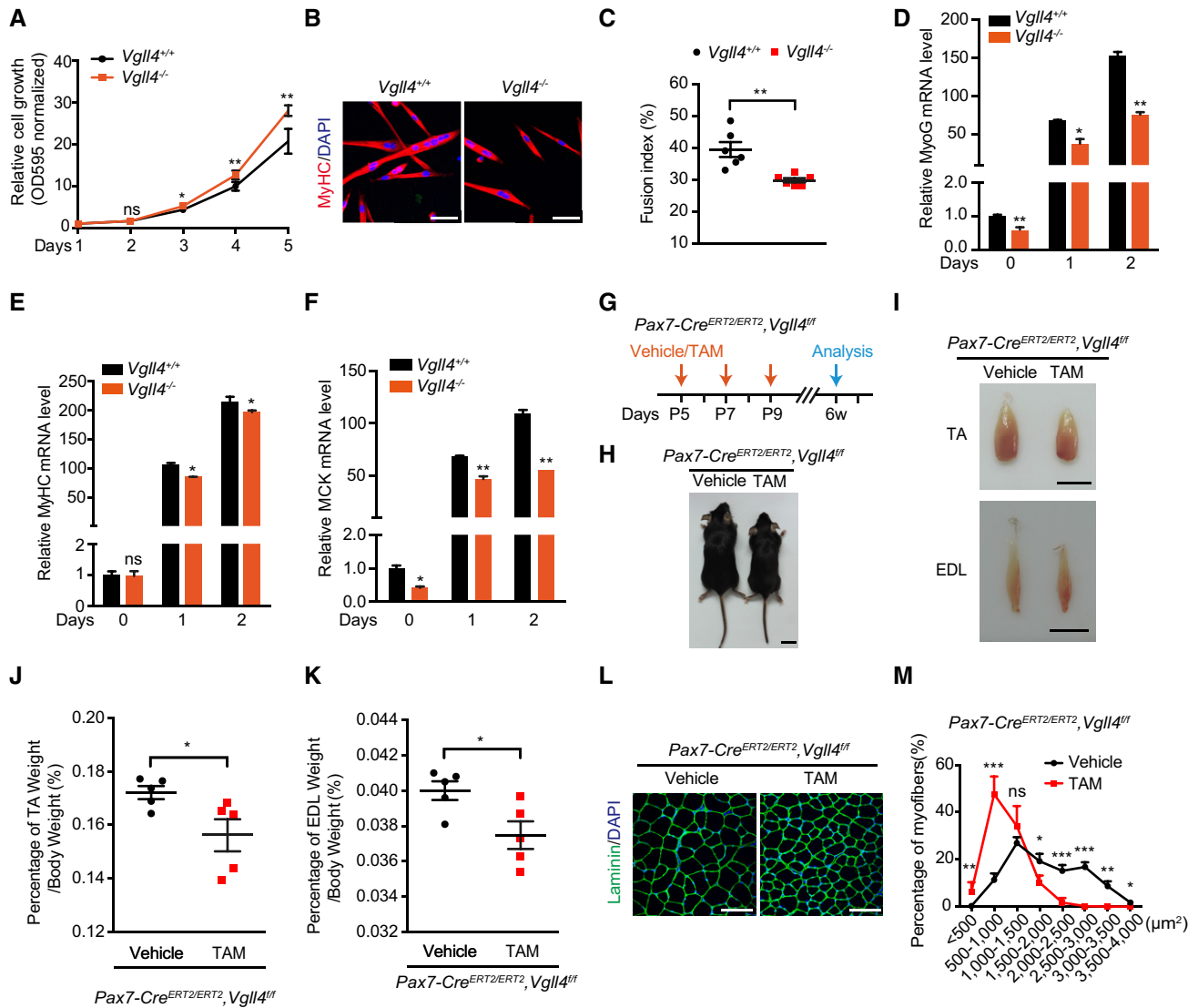
Figure 2. VGLL4 plays essential roles in maintaining the function and homeostasis of MuSCs.

A The proliferation rates of MuSCs sorted from 12 weeks of age of $Vgll4^{+/+}$ and $Vgll4^{-/-}$ mice were detected by MTT assay. The absorbance was measured at the wavelengths of 595 and 630 nm. Five repeats per group.

B Representative immunostaining of MyHC for cultured MuSCs from 12 weeks of age of $Vgll4^{+/+}$ and $Vgll4^{-/-}$ mice at 2 days of differentiation. Scale bars: 50 μm.

C Fusion index of MyHC$^+$ myotubes in MuSCs-derived myoblasts from 12 weeks of age of $Vgll4^{+/+}$ and $Vgll4^{-/-}$ mice. Cells were collected at 2 days post-differentiation. Each MuSC population was isolated from one mouse. One slide was made for each MuSC population. Two views of photographs were taken from each slide. n = 6 views from 3 mice per group.

D–F mRNA level of MyoG (D), MyHC (E), and MCK (F) during differentiation of MuSCs from 12 weeks of age of $Vgll4^{+/+}$ and $Vgll4^{-/-}$ mice. Cells were cultured and collected at 0, 1, and 2 days of differentiation, respectively. Data were calculated from three independent replicates.

G The schematic strategy for intraperitoneal injection of sunflower oil (vehicle) or tamoxifen (TAM) in $Pax7$-$cre^{ERT2/ERT2}$,$Vgll4^{f/f}$ mice. TAM was injected intraperitoneally for three times every second day to induce depletion of VGLL4 at postnatal day 5 (P5). Mice with sunflower oil injection were considered as control mice. All mice were analyzed at 6 weeks.

H Representative photographs of $Pax7$-$cre^{ERT2/ERT2}$,$Vgll4^{f/f}$ mice treated with vehicle or TAM at 6 weeks of age. Scale bars: 1 cm.

I Representative photographs of the TA and EDL muscles from $Pax7$-$cre^{ERT2/ERT2}$,$Vgll4^{f/f}$ mice treated with vehicle or TAM at 6 weeks of age. Scale bars: 5 mm.

J Ratio analysis of TA muscle weight to the whole body weight from $Pax7$-$cre^{ERT2/ERT2}$,$Vgll4^{f/f}$ mice treated with vehicle or TAM at 6 weeks of age (n = 5 mice).

K Ratio analysis of EDL muscle weight to the whole body weight from $Pax7$-$cre^{ERT2/ERT2}$,$Vgll4^{f/f}$ mice treated with vehicle or TAM at 6 weeks of age (n = 5 mice).

L Representative immunostaining for Laminin (green) and DAPI (blue) of TA muscles' maximum cross-sections from $Pax7$-$cre^{ERT2/ERT2}$,$Vgll4^{f/f}$ mice treated with vehicle or TAM at 6 weeks of age. Scale bars: 100 μm.

M Percentage distribution of myofibers in TA muscles' maximum cross-sectional area derived from $Pax7$-$cre^{ERT2/ERT2}$,$Vgll4^{f/f}$ mice treated with vehicle or TAM at 6 weeks of age (n = 6 mice).

Data information: In (A, C–F, J, K, M), data were presented as mean ± SEM; *P < 0.05, **P < 0.01, ***P < 0.001, ns: no significance; unpaired Student t-test.

GFP is fused to the C-terminus of VGLL4 (Yu *et al*, 2019). In order to check whether VGLL4 expression peaks in MuSCs, we performed co-staining of Pax7 and GFP in TA muscles. The results revealed that VGLL4 expression was increased in MuSCs (Pax7⁺) and other cell types (Pax7⁻) in response to muscle injury (Fig EV3A). We also performed co-staining of MyHC and GFP, and the results suggested that VGLL4 expression was increased in fibers (MyHC⁺) as well (Fig EV3B). Meanwhile, we quantified VGLL4 mRNA level in TA muscles of $Pax7\text{-}Cre^{ERT2/ERT2}$,$Vgll4^{f/f}$ mice during muscle regeneration. The similar trend of VGLL4 mRNA level was observed in MuSCs-specific VGLL4 knockout mice compared with the control mice during muscle regeneration (Fig EV3C). These results together imply that the expression of VGLL4 not only up-regulates in the MuSCs but also in other types of muscle cells during muscle regeneration. We next checked whether VGLL4 expression is up-regulated in myoblasts *in vitro*. During C2C12 myoblast differentiation, VGLL4 expression temporarily increased at both mRNA and protein levels (Fig EV3D and E). Collectively, these results suggest that VGLL4 expression is quickly induced in response to muscle injury and then gradually declined during muscle regeneration, indicating that VGLL4 plays a potential role in muscle regeneration.

In response to muscle injury, MuSCs undergo massive proliferation and then differentiation to form myotubes that replace the damaged myofibers (Comai & Tajbakhsh, 2014). To investigate the function of VGLL4 in muscle regeneration, we first examined the effect of VGLL4 on MuSCs proliferation in adult $Pax7\text{-}Cre^{ERT2/ERT2}$, $Vgll4^{f/f}$ mice (Fig 3D). Muscle injury was induced by cardiotoxin (CTX) injection to TA muscles. More proliferative cells especially MuSCs were observed in MuSCs-specific VGLL4 knockout mice post-injury, suggesting that VGLL4 impairs cell proliferation in general (Figs 3E and F, and EV3F). Previous studies have shown that VGLL4 acts as an antagonist of YAP by directly competing with YAP for binding to TEAD4 (Guo *et al*, 2013; Koontz *et al*, 2013; Jiao *et al*, 2014). To define whether VGLL4 inhibits MuSCs proliferation through disrupting YAP-TEAD4 complex, we performed immunoprecipitation assay in C2C12 myoblasts. We found that more YAP was precipitated by TEAD4 in VGLL4 knockdown C2C12 cells (Fig 3G). We then quantified the expression levels of YAP target genes. Notably, the expression levels of CTGF and CYR61 showed reverse tendency with VGLL4 expression level in MuSCs at the initiation of differentiation (Fig 3H). We next performed TEAD4 reporter assay to analyze YAP-TEAD downstream target gene expression (Zhao *et al*, 2008) and found that VGLL4 overexpression inhibited YAP-induced TEAD4 reporter activity in C2C12 cells (Fig EV3G). Moreover, inactivation of VGLL4 increased expression levels of YAP target genes in MuSCs (Fig 3I). Consistently, VGLL4 knockdown increased the expression levels of YAP target genes in C2C12 cells (Fig EV3H and I). To further confirm that VGLL4-mediated inhibition of MuSCs proliferation is dependent on YAP activity, we generated MuSCs-specific VGLL4 and YAP double-knockout mice in which VGLL4 and YAP were depleted at both mRNA and protein levels in MuSCs (Fig EV3J and K). We found that YAP knockout inhibited MuSCs proliferation and significantly reversed the hyper proliferation of MuSCs induced by VGLL4 knockout (Fig 3J and K).

VGLL4 promotes myoblast differentiation during muscle regeneration

We next assayed whether deficiency of VGLL4 in MuSCs affects MuSCs-derived myoblast differentiation during muscle regeneration. We observed that MuSCs-specific VGLL4 knockout mice displayed regeneration defects as indicated by smaller myofiber size at 3, 5, and 7 days post-injury (Figs 4A and B, and EV4A–C). In addition, knockout of VGLL4 in MuSCs resulted in decreased expression levels of MyoG, MyHC, and MCK at 5 days post-injury in TA muscles (Fig 4C and D). The expression level of MyoG was also decreased in cultured MuSCs during differentiation (Fig 4E). Taken together, although depletion of VGLL4 enhanced MuSCs proliferation, it impaired myoblast differentiation, implying the dual roles of VGLL4 in the process of muscle regeneration. Consistent with our *in vivo* results, knockdown of VGLL4 by siRNA dramatically impaired myoblast fusion and myotube formation in C2C12 cells (Figs 4F and G, and EV4D and E). Furthermore, silencing of VGLL4 led to a potent reduction in MyoG, MyHC, and MCK expression levels (Figs 4H and I, and EV4F–J). In contrast, VGLL4 overexpression dramatically enhanced myoblasts differentiation (Fig 4J and K). Consistently, expression levels of MyoG, MyHC, and MCK were up-regulated in VGLL4 overexpression myoblasts (Figs 4L and M, and EV4K and L). Taken together, these data demonstrate that VGLL4 promotes myoblast differentiation.

VGLL4 promotes MyoG expression and myoblast differentiation via TEAD4

Having observed that MyoG expression was tightly regulated by VGLL4 both *in vitro* and *in vivo*, we next investigated how VGLL4 regulates MyoG transcription. Since VGLL4 does not contain DNA-binding domain, we then examined whether TEAD transcription factors (TEAD1-4) are required in this process. During both muscle regeneration and C2C12 cell differentiation, we found that TEAD4 shared the same expression profile with VGLL4 not only at transcription level but also at protein level (Figs 5A and B, and EV5A–D). To further confirm the role of TEAD4 in myogenesis, we performed RNAi against TEAD4 in C2C12 myoblasts. TEAD4 knockdown led to impaired cell differentiation (Fig EV5E–H). Consistent with the morphology change, MyoG expression was down-regulated after TEAD4 knockdown (Fig EV5I and J). It has been reported that VGLL4 directly interacts with TEAD4 via TDU domains (Fig 5C; Chen *et al*, 2004; Koontz *et al*, 2013; Jiao *et al*, 2014). We found that VGLL4-ΔTDU overexpression failed to promote myoblast differentiation compare with wild-type VGLL4 overexpression (Fig 5D and E). Consistent with the morphological changes, the expression levels of MyoG and MyHC were also significantly lower in differentiating myoblasts with VGLL4-ΔTDU overexpression compared with VGLL4 overexpression (Fig 5F). VGLL4-HF4A mutant could disrupt VGLL4-TEAD4 complex formation (Jiao *et al*, 2014). Similar to VGLL4-ΔTDU, we found that VGLL4-HF4A overexpression could not enhance MyoG expression (Fig 5G), indicating that TDU domains-mediated interaction between VGLL4 and TEAD4 is required for MyoG activation and myoblast differentiation. To further check whether TEAD4 is required for the function of VGLL4 in myoblast differentiation, we knocked down TEAD4 in VGLL4 overexpression cells and found that TEAD4 knockdown blocked VGLL4-induced
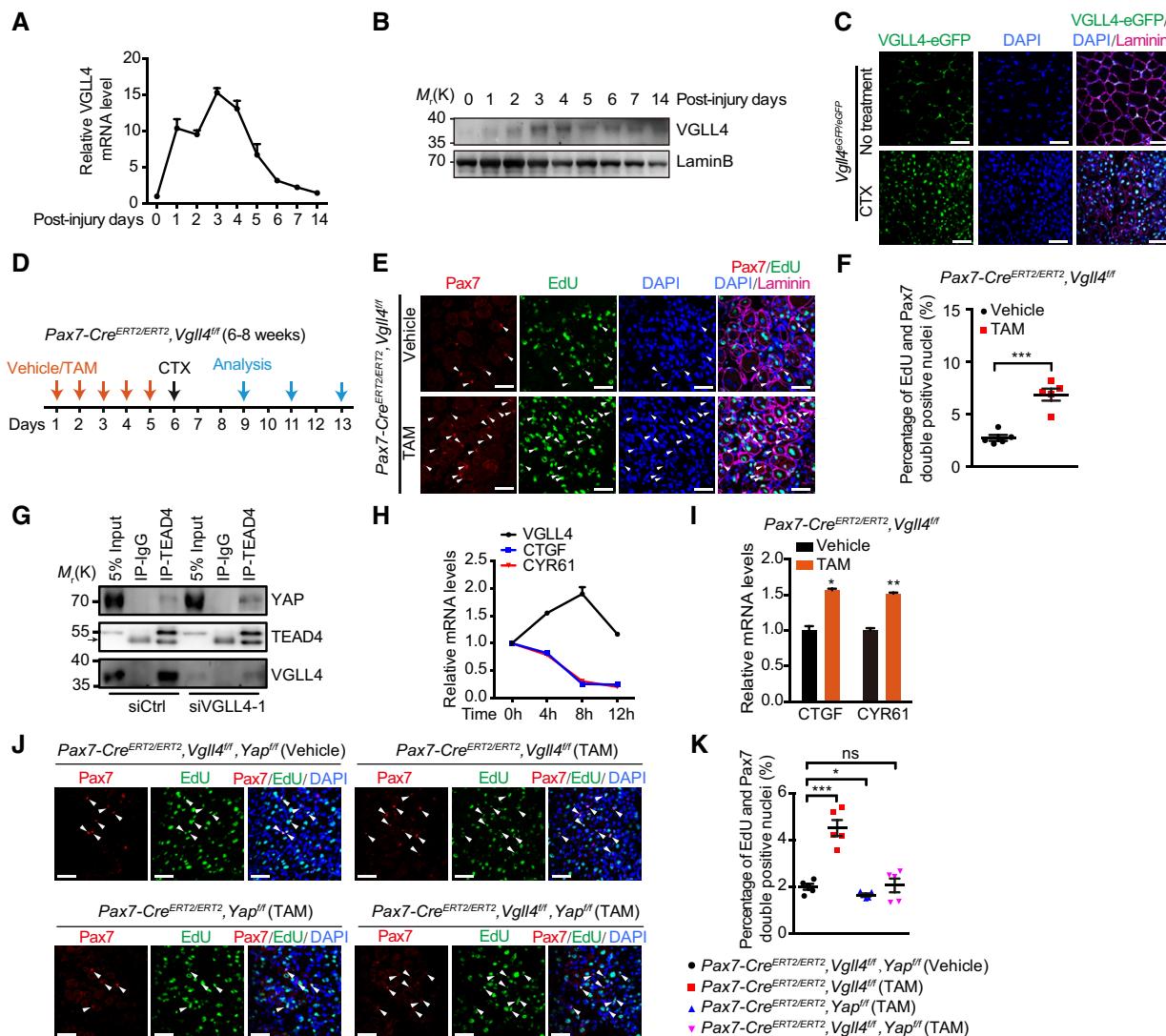
Figure 3. VGLL4 is quickly up-regulated in response to muscle injury and represses MuSCs proliferation via antagonizing YAP activity.

A   VGLL4 mRNA level was measured by RT–qPCR in C57BL/6J mice TA muscles. Samples were collected from cardiotoxin (CTX)-injected TA muscles at 0, 1, 2, 3, 4, 5, 6, 7, 14 days post-injury (n = 6 mice).

B   Immunoblotting showed the expression profile of VGLL4 during muscle regeneration in C57BL/6J mice TA muscles. Samples were collected from CTX-injected TA muscles at 0, 1, 2, 3, 4, 5, 6, 7, 14 days post-injury. Lamin B was used as a loading control.

C   Representative immunostaining for VGLL4-eGFP (green), DAPI (blue), and Laminin (purple) in TA muscles' cross-sections. TA muscles were dissected from 8 weeks of age of $Vgll4^{eGFP/eGFP}$ without treatment or injured $Vgll4^{eGFP/eGFP}$ mice at 5 days post-injury. Scale bars: 50 μm.

D   The schematic strategy for treatment of TAM and CTX in $Pax7\text{-}Cre^{ERT2/ERT2},Vgll4^{f/f}$ mice. Sunflower oil (vehicle) or TAM was first injected intraperitoneally for 5 consecutive days. Muscle injury was next induced by CTX injection to TA muscles. EdU was injected intraperitoneally for two consecutive days before muscle harvest.

E   Representative immunostaining for Pax7 (red), EdU (green), Laminin (purple), and DAPI (blue) of TA muscles' cross-sections from $Pax7\text{-}cre^{ERT2/ERT2},Vgll4^{f/f}$ mice. Mice were analyzed at 5 days post-injury. Arrows represent Pax7 and EdU double-positive nuclei. Scale bars: 50 μm.

F   Quantification of the ratio of proliferative MuSCs with EdU and Pax7 double-positive nuclei from $Pax7\text{-}cre^{ERT2/ERT2},Vgll4^{f/f}$ mice treated with vehicle or TAM at 5 days post-injury. n = 5 mice per group.

G   Endogenous YAP was immunoprecipitated by TEAD4 in HA-TEAD4 overexpression C2C12 cells. C2C12 cells were transfected with either control siRNA (siCtrl) or VGLL4 siRNA (siVGLL4-1). The arrow indicates IgG chain.

H   Relative mRNA levels of VGLL4, CTGF, and CYR61 were measured by RT–qPCR during MuSCs differentiation at different time points. MuSCs were isolated from C57BL/6J mice. Two replicates per group.

I   Relative mRNA levels of CTGF and CYR61 were measured by RT–qPCR. MuSCs were isolated from $Pax7\text{-}cre^{ERT2/ERT2},Vgll4^{f/f}$ mice treated with vehicle or TAM at 5 days post-injury.

J   Representative immunostaining for Pax7 (red), EdU (green), and DAPI (blue) of TA muscles' cross-sections. Mice were analyzed at 5 days post-injury. Arrows represent Pax7 and EdU double-positive nuclei. Scale bars: 50 μm.

K   Quantification of the ratio of proliferative MuSCs with EdU and Pax7 double-positive nuclei from the indicated mice at 5 days post-injury. n = 5 mice per group.

Data information: In (A, F, H, I, K), data were presented as mean ± SEM; *P < 0.05, **P < 0.01, ***P < 0.001, ns: no significance; unpaired Student t-test.
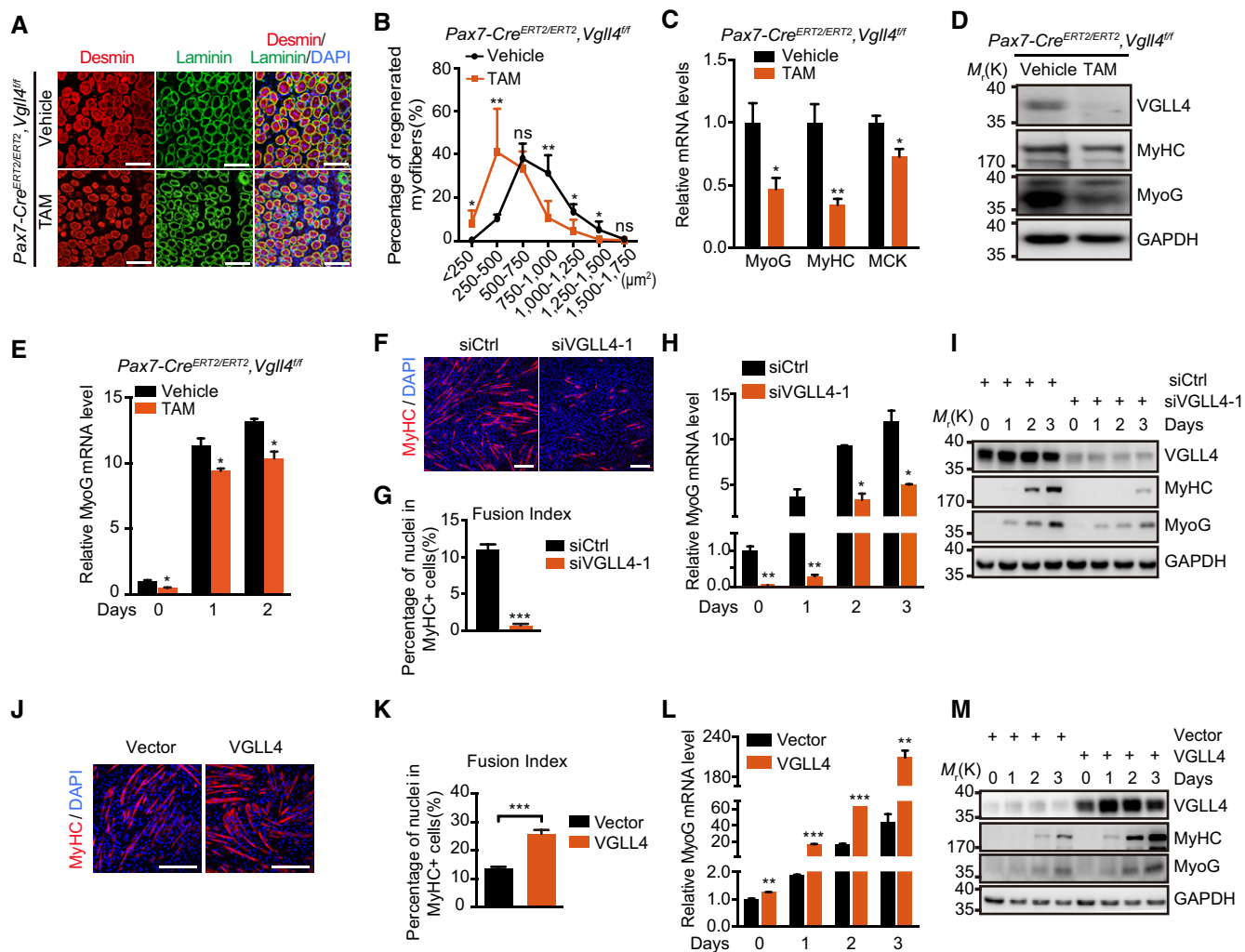
Figure 4. VGLL4 promotes myoblast differentiation during muscle regeneration.

A   Representative immunostaining for Desmin (red), Laminin (green), and DAPI (blue) of TA muscles' cross-sections from *Pax7-cre^ERT2/ERT2*,*Vgll4^f/f* mice with or without TAM treatment. Mice were analyzed at 5 days post-injury. Scale bars: 100 μm.

B   Percentage distribution of regenerated myofibers (with central nuclei) in TA muscles' maximum cross-sectional area derived from *Pax7-cre^ERT2/ERT2*,*Vgll4^f/f* mice with or without TAM treatment at 5 days post-injury. Vehicle: *n* = 5 mice, TAM: *n* = 6 mice.

C   Relative mRNA levels of myogenic markers in TA muscles from *Pax7-cre^ERT2/ERT2*,*Vgll4^f/f* mice with or without TAM treatment. TA muscles were analyzed at 5 days post-injury (*n* = 4 mice per group).

D   Immunoblotting showed the expressions of the indicated proteins in injured TA muscles from *Pax7-cre^ERT2/ERT2*,*Vgll4^f/f* mice with or without TAM treatment. TA muscles were analyzed at 5 days post-injury. GAPDH was used as a loading control.

E   mRNA level of MyoG during differentiation of MuSCs from *Pax7-cre^ERT2/ERT2*,*Vgll4^f/f* mice with or without TAM treatment. Cells were cultured and collected at 0, 1, and 2 days of differentiation, respectively. Data were calculated from three independent replicates.

F   Representative MyHC staining for control (siCtrl) and VGLL4 RNAi (siVGLL4-1) myoblasts at 3 days of differentiation. Control or VGLL4 siRNAs were transfected into myoblast cells for 48 h before the initiation of differentiation. Scale bars: 50 μm.

G   Quantification of the fusion index from C2C12 myoblasts with siCtrl or siVGLL4-1 transfection. Cells were collected at 3 days of cell differentiation. Data were calculated from three independent replicates.

H   Knockdown of VGLL4 down-regulates the transcriptional level of MyoG. Cells were collected at 0, 1, 2, and 3 days post-differentiation, respectively. Data were calculated from three independent replicates.

I   Immunoblotting showed the expressions of the indicated proteins in control or VGLL4 knockdown C2C12 cells. Cells were collected at 0, 1, 2, and 3 days post-differentiation, respectively. GAPDH was used as a loading control.

J   Representative MyHC staining for control and VGLL4 overexpression myoblasts at 3 days of differentiation. C2C12 cells were infected by lentivirus-encoding pLEX-HA vector or HA-VGLL4 and then induced for differentiation. Scale bars: 50 μm.

K   Quantification of the fusion index from C2C12 myoblasts with pLEX-HA vector or HA-VGLL4 overexpression. Cells were collected at 3 days of cell differentiation. Data were calculated from three independent replicates.

L   VGLL4 overexpression up-regulates the transcriptional level of MyoG. Cells were collected at 0, 1, 2, and 3 days post-differentiation, respectively. Data were calculated from three independent replicates.

M   Immunoblotting showed the expressions of the indicated proteins in control or VGLL4 overexpression C2C12 cells. Cells were collected at 0, 1, 2, and 3 days post-differentiation, respectively. GAPDH was used as a loading control.

Data information: In (B, C, E, G, H, K, L), data were presented as mean ± SEM; *P < 0.05, **P < 0.01, ***P < 0.001, ns: no significance; unpaired Student *t*-test.
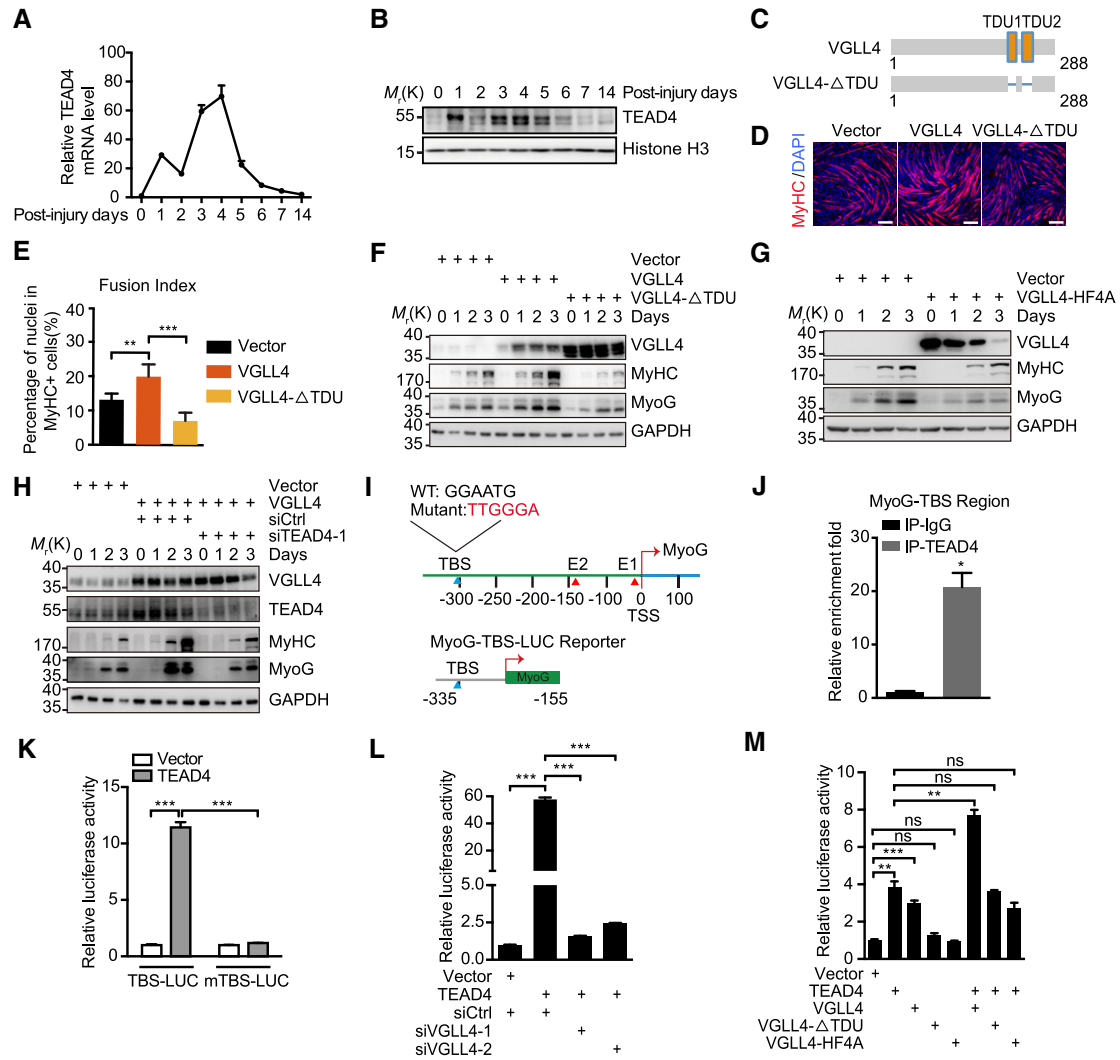
Figure 5. VGLL4 acts as a co-activator of TEAD4 to promote MyoG transactivation and myoblast differentiation.

A TEAD4 mRNA level was measured by RT–qPCR in C57BL/6J mice's TA muscles during muscle regeneration. Samples were collected from CTX-injected TA muscles at 0, 1, 2, 3, 4, 5, 6, 7, and 14 days post-injury (*n* = 6 mice).

B Immunoblotting showed the expression profiles of TEAD4 during muscle regeneration. Samples were collected from CTX-injected TA muscles at 0, 1, 2, 3, 4, 5, 6, 7, and 14 days post-injury. Histone H3 was used as a loading control.

C Schematic illustration of the domain organization for mouse VGLL4 and VGLL4-ΔTDU.

D Representative MyHC staining of C2C12 myoblasts with control, VGLL4, or VGLL4-ΔTDU overexpression at 3 days post-differentiation. Scale bars: 50 μm.

E Quantification of the fusion index from C2C12 myoblasts with control, VGLL4, or VGLL4-ΔTDU overexpression at 3 days post-differentiation. Data were calculated from three independent replicates.

F VGLL4-ΔTDU overexpression inhibits the up-regulation of MyoG and MyHC in VGLL4 overexpression C2C12 cells. Cells were collected at 0, 1, 2, and 3 days of differentiation, respectively. GAPDH was used as a loading control.

G VGLL4-HF4A overexpression inhibits myogenesis of myoblasts. C2C12 cells were collected at 0, 1, 2, and 3 days of differentiation, respectively. GAPDH was used as a loading control.

H Knockdown of TEAD4 blocks the increased expression levels of MyoG and MyHC induced by VGLL4 overexpression during myoblasts differentiation. C2C12 cells were collected at 0, 1, 2, and 3 days of differentiation, respectively. GAPDH was used as a loading control.

I Schematic illustration of the core promoter structure of MyoG with potential TEAD4 binding site (TBS). The wild-type and TBS mutant sequences are indicated. E1 and E2 represent MyoG E1 and E2 box recognized by MyoD. TSS represents the transcription start site in MyoG promoter (Heidt *et al*, 2007). The promoter region (−335 to −155) cloned for MyoG-TBS luciferase (MyoG-TBS-LUC) is indicated.

J ChIP analysis of TEAD4 on MyoG-TBS promoter region was performed in HA-TEAD4 overexpression C2C12 cells. Data were calculated from two independent replicates.

K Luciferase analysis showed the effects of TEAD4 on wild-type MyoG-TBS luciferase (TBS-LUC) or mutant MyoG-TBS luciferase (mTBS-LUC). C2C12 cells were collected at 1 day post-differentiation. Data were calculated from three independent replicates.

L Luciferase analysis showed the effects of VGLL4 RNAi on TEAD4-induced MyoG-TBS luciferase activity (MyoG-TBS-LUC). C2C12 cells were collected at 1 day post-differentiation. Data were calculated from three independent replicates.

M Luciferase analysis showed the effects of VGLL4-ΔTDU and VGLL4-HF4A on MyoG-TBS-LUC with or without TEAD4 overexpression. C2C12 cells were collected at 1 day post-differentiation. Data were calculated from three independent replicates.

Data information: In (A, E, J–M), data were presented as mean ± SEM; *$P < 0.05$, **$P < 0.01$, ***$P < 0.001$, ns: no significance; unpaired Student *t*-test.

up-regulation of MyoG (Figs 5H and EV5K). These results suggest that the function of VGLL4 in promoting myoblast differentiation mainly depends on TEAD4.

We next examined how VGLL4-TEAD4 regulates myoblast differentiation. We characterized a conserved TEAD binding site "GGAATG" (TBS) in the promoter region of MyoG, which is close to MyoD binding E-box region (E1 and E2; Fig 5I). We then performed TEAD4 chromatin immunoprecipitation (ChIP) assay, and the ChIP-qPCR results indicated that TEAD4 bound to the conserved TBS in MyoG promoter (Fig 5J). Two luciferase reporters driven by wild-type MyoG promoter and TBS mutant MyoG promoter were generated as shown in Fig 5I. TEAD4 overexpression significantly enhanced wild-type MyoG promoter-reporter activity but had no effect on the mutant MyoG promoter-reporter activity (Fig 5K). In addition, VGLL4 knockdown repressed TEAD4-induced MyoG transcriptional activity (Fig 5L). Overexpression of VGLL4 could further increase TEAD4-induced MyoG transcriptional activity, and such enhancement was dependent on VGLL4-TEAD4 interaction since VGLL4-ΔTDU and VGLL4-HF4A failed to increase TEAD4-induced MyoG transcriptional activity (Fig 5M). These data imply that VGLL4 functions as a co-activator of TEAD4 to promote MyoG trans-activation and myoblast differentiation.

VGLL4 enhances the interaction between TEAD4 and MyoD to achieve efficient MyoG activation

MyoD is the master regulator of myogenesis, and the presence of certain binding sites paired with the E-box region could confer promoter-specific activity to MyoD (Tapscott, 2005). We noticed that in the promoter of MyoG, TEAD4 binding region was close to MyoD binding region. To elucidate the correlation between TEAD4 and MyoD, we constructed a luciferase reporter driven by MyoG promoter containing both TBS and E-box regions. The mutant MyoG promoter-luciferase reporter containing mutant TBS and wild-type E-box regions was also generated (Fig 6A). MyoD recognized the conserved E-box sequences in MyoG promoter region and activated MyoG promoter-reporter activity (Fig 6B). TEAD4 overexpression significantly increased MyoD-induced MyoG transcriptional activity. However, when the TEAD binding site was mutated in MyoG promoter-reporter, TEAD4 overexpression had no effect on MyoG transcriptional activity (Fig 6B), suggesting that the synergistic effect of TEAD4 and MyoD on MyoG transcription is required for TEAD4's binding to its own recognizing site. We then did co-immunoprecipitation assay, and the results revealed that TEAD4 could pull down endogenous MyoD in C2C12 cells (Fig 6C). GST pull-down assay further confirmed the interaction between TEAD4 and MyoD (Figs 6D and EV5L). TEAD4 is constituted of an N-terminal TEA domain and a C-terminal YAP-binding domain (YBD; Fig 6E; Shi *et al*, 2017). YBD domain of TEAD4 can directly interact with YAP/TAZ and VGLL4 proteins, whereas the TEA domain of TEAD4 is responsible for binding DNA (Shi *et al*, 2017). Based on the structure of TEAD4, we truncated TEAD4 into N-terminal (TEAD4-N, 1-216AA) and C-terminal (TEAD4-C, 217-434AA) to determine the region in TEAD4 that interacts with MyoD (Fig 6E). GST-MyoD protein was capable of pulling down full-length and TEA domain containing N-terminal fragment of TEAD4, but not the C-terminal fragment of TEAD4 (Fig 6F). We further checked the function of TEAD4-N and TEAD4-C on myoblast differentiation. Myoblast cells

with TEAD4-N overexpression showed higher fusion index and higher expression levels of MyoG, MyHC, and MCK compared with TEAD4-C overexpression, indicating better differentiation ability of myoblasts with TEAD4-N overexpression (Fig EV5M–Q). Direct interaction between purified TEA domain and MyoD proteins was confirmed by pull-down assay (Fig 6G). By mutagenesis screening, we further identified a mutation of TEAD4-TEA (Q103A, V104R) that abolished TEAD4-MyoD interaction, suggesting that Q103 and V104 in TEA domain are responsible for TEAD4 and MyoD interaction (Fig 6G). We next examined whether there is protein–protein interaction between MyoD and VGLL4. GST pull-down experiments showed that VGLL4 could be indirectly pulled down by GST-MyoD in the presence of TEAD4 (Fig 6H). Interestingly, VGLL4 enhanced the interaction between TEAD4 and MyoD in a dosage-dependent manner (Fig 6I). It is noteworthy that TEAD4 increased MyoG transcriptional activity in MyoD overexpression cells, and such effect could be further enhanced by VGLL4 overexpression (Fig 6J). In order to investigate whether VGLL4-TEAD4 is required for MyoD activity, we knocked down TEAD4 or VGLL4 in MyoD overexpression myoblasts, which leads to inhibition of MyoD-induced MyoG expression (Fig EV5R and S). In conclusion, these results suggest that VGLL4 cooperates with TEAD4 and MyoD to efficiently activate MyoG transcription during myoblast differentiation.

Collectively, data gathered in this study clarify the role of VGLL4 in maintaining the balance between muscle stem cells proliferation and differentiation at different stages of muscle regeneration. At the early stage of muscle regeneration, VGLL4 functions as a conventional YAP repressor to inhibit YAP-mediated transcription and MuSCs proliferation. At the late stage of muscle regeneration, VGLL4 functions as an indispensible co-activator of TEAD4 and enhances the interaction between TEAD4 and MyoD. The VGLL4-TEAD4-MyoD transcriptional complex further drives the expression of MyoG to initiate MuSCs differentiation (Fig 6K).

Discussion

In myoblasts, as in a variety of cell types, cell proliferation and cell differentiation are controlled by a balance of opposing cellular signals. Skeletal muscle regeneration is a highly orchestrated process. Muscle satellite cells (MuSCs) are the adult stem cells that regenerate skeletal muscles in response to muscle injury (Brack & Rando, 2012; Yin *et al*, 2013). MuSCs undergo cell proliferation and differentiation to achieve timely regeneration (Seale & Rudnicki, 2000). VGLL4, a new member of the Hippo pathway, is intensively investigated in inhibition of cell proliferation by competing with YAP to bind TEADs, but its role in MuSCs proliferation and differentiation during muscle regeneration remains unclear. In this study, we identified that VGLL4 plays dual roles in skeletal muscle regeneration. MuSCs-specific VGLL4 knockout mice displayed two obvious muscle phenotypes: increased MuSCs proliferation and impaired MuSCs differentiation, which ultimately resulted in muscle regeneration defects. Our work demonstrates that VGLL4 functions from a repressor to an activator in muscle regeneration, which sheds light on the role of VGLL4 in skeletal muscle regeneration.

It is reported that activation of YAP promotes proliferation of activated muscle progenitor cells and MuSCs-derived myoblasts (Judson *et al*, 2012). YAP activity is inhibited by VGLL4, which is
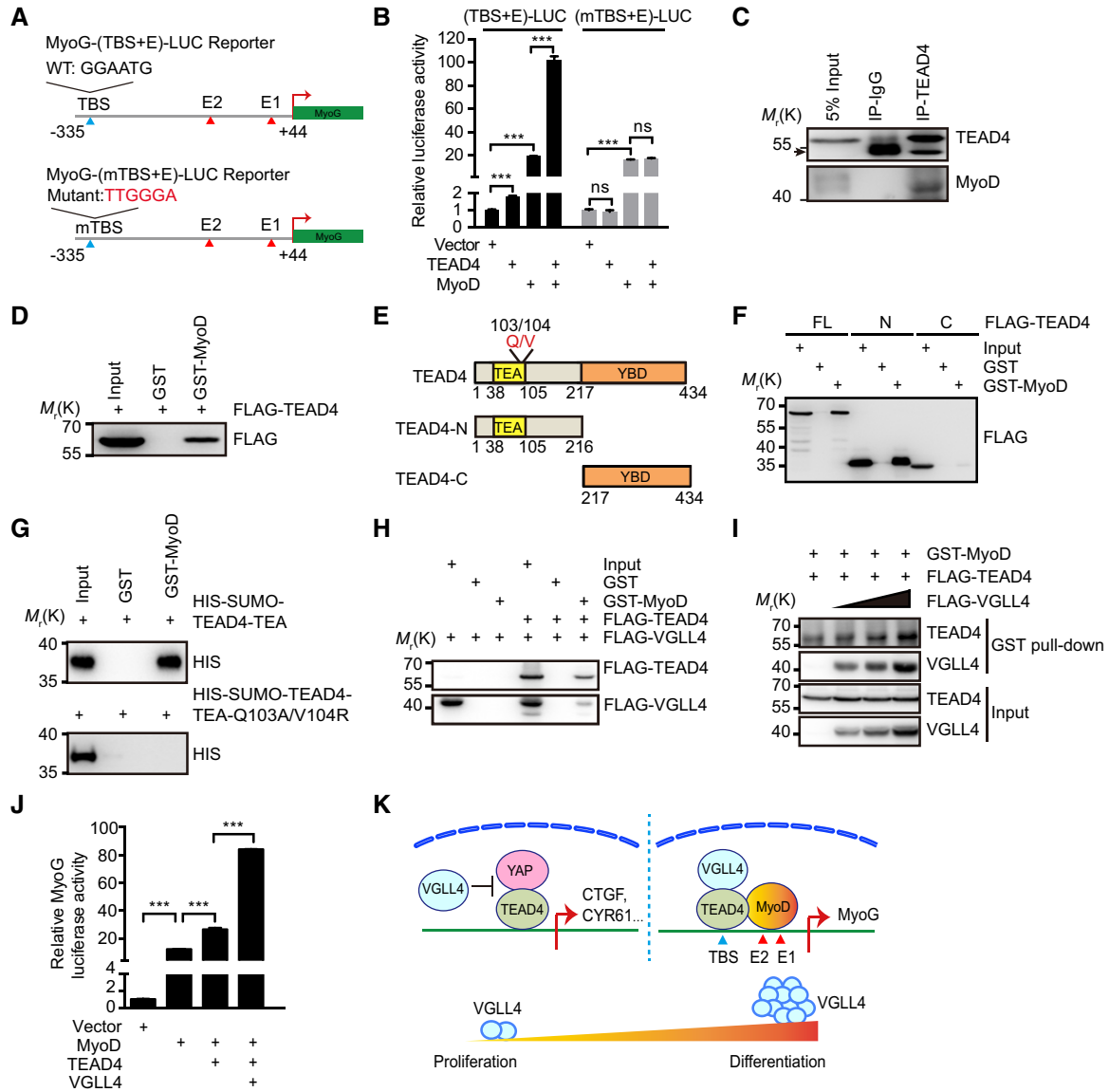
Figure 6. VGLL4 enhances the interaction between TEAD4 and MyoD to achieve efficient MyoG activation.

A   Schematic illustration of the promoter region (−335 to +44) cloned for MyoG luciferase reporter containing both TBS and E-box regions. TBS: TEAD4 binding site. E1 and E2 represent E-box region recognized by MyoD, respectively.

B   Luciferase analysis showed the effects of MyoD and TEAD4 on wild-type MyoG luciferase reporter containing wild-type TBS and E-box sequences ((TBS+E)-LUC) or mutant MyoG luciferase reporter containing mutant TBS and wild-type E-box sequences ((mTBS+E)-LUC). Cells were collected at 1 day post-differentiation. Data were calculated from three independent replicates.

C   Co-immunoprecipitation of TEAD4 and endogenous MyoD in HA-TEAD4 overexpression C2C12 cells. The arrow indicates IgG chain.

D   GST pull-down assay showed the interaction between MyoD and TEAD4. Cell lysates from FLAG-TEAD4 overexpression 293T cells were incubated with recombinant GST or GST-MyoD protein.

E   Schematic illustration of the domain organization for human TEAD4, TEAD4-N/C mutations and two amino acids (Q103 and V104) responsible for TEAD4's interaction with MyoD.

F   GST pull-down analysis between MyoD and various TEAD4 mutants. FL: full length. N: TEAD4 N-terminal domain. C: TEAD4 C-terminal domain.

G   GST pull-down analysis between purified GST-MyoD and HIS-SUMO-TEAD4-TEA or HIS-SUMO-TEAD4-TEA-Q103A/V104R mutant proteins.

H   Lysates from 293T cells with FLAG-tagged VGLL4 and TEAD4 expressions were incubated with recombinant GST or GST-MyoD protein. GST pull-down assay shows the indirect binding between VGLL4 and MyoD that is mediated by TEAD4.

I   Lysates from 293T cells with FLAG-tagged VGLL4 and TEAD4 expressions were incubated with recombinant GST-MyoD protein. GST pull-down assay shows that VGLL4 enhances TEAD4 and MyoD interaction in a dosage-dependent manner.

J   VGLL4, TEAD4, and MyoD synergistically activate (TBS+E)-LUC. C2C12 cells were collected at 1 day post-differentiation. Data were calculated from three independent replicates.

K   A model of how VGLL4 regulates myoblast proliferation and differentiation. TBS represents TEAD4 binding site. E1 and E2 represent MyoG E1 and E2 box recognized by MyoD.

Data information: In (B and J), data were presented as mean ± SEM; ***$P < 0.001$, ns: no significance; unpaired Student *t*-test.

due to disrupting of the YAP-TEAD4 complex formation (Jiao *et al*, 2014; Zhang *et al*, 2014). Consistently, the expression levels of the Hippo pathway target genes were increased in VGLL4 knockout MuSCs. Therefore, at the early stage of muscle regeneration, inactivation of VGLL4 allows the stable existence of YAP-TEAD4 complex to promote myoblast proliferation. Recent studies revealed that VGLL4 is also involved in Wnt/β-catenin signaling (Jiao *et al*, 2017) and Rho/Rock pathway (Tajonar *et al*, 2013), suggesting that VGLL4 may achieve its functions by multiple aspects. It will be interesting to understand how multiple mechanisms work together to achieve the function of VGLL4 in skeletal muscles.

Previous study has revealed that TEAD4 mutant mice displayed delayed muscle regeneration after injury (Joshi *et al*, 2017), which is similar with the phenotype observed in VGLL4 knockout mice. Our study showed that TEAD4 acts as a main binding partner of VGLL4 in regulating muscle differentiation. TEADs are originally identified to recognize and bind MCAT elements (Davidson *et al*, 1988). MCAT elements have been identified in the promoter or enhancer region of muscle-specific genes (Davidson *et al*, 1988; Anbanandam *et al*, 2006). We identified that TEAD4 directly binds to the classical MCAT site (TEAD binding site) in MyoG promoter and VGLL4 functions as a co-activator of TEAD4 to promote MyoG expression. In addition to the TEAD4 binding site close to MyoD binding E-box region that is mentioned in this study, we noticed that there are several other potential TEAD4 binding sites in MyoG promoter region. It is possible that VGLL4/TEAD4 can bind to the other potential TEAD4 binding sites, which is required for further investigation. We demonstrated that loss of VGLL4 resulted in lower MyoG, MyHC, and MCK expression levels both *in vivo* and *in vitro*. Here, the expression levels of the terminal differentiation markers MyHC and MCK are used as the readout for MyoG activity. MyHC promoter also contains several MCAT TEAD binding elements (Stewart *et al*, 1998), which raised the possibility that MyHC is regulated both by MyoG and TEAD4 in VGLL4 knockdown or knockout myoblasts. It is interesting to investigate whether the similar mechanism can be applied to MyHC transcription regulation and to identify whether TEAD4/VGLL4 work together with MyoG to activate MyHC transcription in the future.

MyoD has been considered to be the master regulator of myogenesis, which can transdifferentiate non-muscle cells to muscle cells (Weintraub *et al*, 1989, 1991; Berkes & Tapscott, 2005). The interaction of MyoD with other factors appears to be necessary for MyoD to activate MyoG transcription. Transcription activators/co-activators such as FoxO3, Rb, CBP, p300, p57, β-catenin, and CTCF have been reported to direct interact with MyoD and enhance its transactivation ability (Yuan *et al*, 1996; Reynaud *et al*, 2000; Polesskaya & Harel-Bellan, 2001; Polesskaya *et al*, 2001; Kim *et al*, 2008; Battistelli *et al*, 2014; Peng *et al*, 2017). Transcription repressors/co-repressors such as Id1, Id2, TLE3, and Suv39h1 interact with MyoD to repress its transcription activation activity (Mal *et al*, 2001; Paulmurugan *et al*, 2002; Mal, 2006; Kokabu *et al*, 2017). Identifying more MyoD interaction partners will help us further understand the mechanism of MyoD-driven transcription. For example, the stable binding of MyoD to the MyoG promoter requires for its interaction with an adjacent protein complex containing the homeodomain proteins Pbx and Meis (Berkes *et al*, 2004). Having observed that VGLL4, TEAD4, and MyoD can synergistically activate MyoG expression, it seems likely that the cooperative heterotypic

interaction of MyoD with its adjacent factors TEAD4/VGLL4 is crucial for establishing a stable and functional transcriptional complex. Though direct binding between TEAD4 and MyoD was detected by *in vitro* pull-down assay, MyoD activity regulated by VGLL4/TEAD4 can also be indirectly affected, which awaits further investigation.

Here, we found that VGLL4 can work in both YAP-dependent and YAP-independent manners to coordinate proliferation and differentiation in myoblasts. At the later stage of muscle regeneration, VGLL4 acts as a co-activator of MyoD by stabilizing MyoD-TEAD4 interaction and plays critical roles in facilitating the initiation of MuSCs differentiation. The synergistically role of VGLL4, TEAD4, and MyoD greatly activates transcription of MyoG and turn on cell differentiation. It seems to be a fast and precise way to regulate myoblast differentiation, which avoids going through the slow and complicated transcription and translation processes.

Our work define the dual roles of VGLL4 in maintaining the balance of MuSCs proliferation and differentiation during muscle regeneration, which may provide a new mechanism to achieve efficient and accurate regulation for muscle regeneration and other well-orchestrated multi-step biological processes. It remains to be determined whether the dual function of VGLL4 in muscle regeneration are regulated by other signaling pathways or other transcriptional factors. If that is the case, how the cooperation is achieved will be another interesting question for further investigation.

Materials and Methods

Mice models

The mice were housed in a specific pathogen-free environment at the Shanghai Institute of Biochemistry and Cell Biology (SIBCB) and treated in strict accordance with protocols approved by the Institutional Animal Care and Use Committee of SIBCB (Approval number: SIBCB-S328-1511-052-C01). Generation of the transgenic *Vgll4*$^{-/-}$ and *Vgll4*$^{f/f}$ mice has been described before (Yu *et al*, 2019). Briefly, *Vgll4* knockout-first mice (*Vgll4*$^{LacZ/+}$) were first generated by the knockout-first strategy as previously described (Skarnes *et al*, 2011). To obtain heterozygous *Vgll4*$^{+/-}$ mice, the male *Vgll4*$^{lacZ/+}$ mice were crossed with female *Sox2*$^{Cre+}$ mice (Hayashi *et al*, 2003). *Vgll4*$^{+/-}$ mice were then intercrossed to generate homozygous *Vgll4*$^{-/-}$ knockout mice. Besides, *Vgll4*$^{lacZ/+}$ mice were crossed with *Flp* mice to obtain heterozygous *Vgll4*$^{f/+}$ mice. *Vgll4*$^{f/+}$ mice were then intercrossed to generate homozygous *Vgll4*$^{f/f}$ conditional knockout mice. *Pax7-Cre*^{ERT2} mice were purchased from Jackson Laboratory. *Yap*$^{f/f}$ mice were kindly provided by Dr. Fernando D Camargo. *Pax7-Cre*^{ERT2} mice were crossed with *Vgll4*$^{f/f}$ mice and *Yap*$^{f/f}$ mice to generate *Pax7-Cre*$^{ERT2/ERT2}$,*Vgll4*$^{f/f}$ (*Vgll4*^{CKO}); *Pax7-Cre*$^{ERT2/ERT2}$,*Yap*$^{f/f}$; and *Pax7-Cre*$^{ERT2/ERT2}$,*Vgll4*$^{f/f}$,*Yap*$^{f/f}$ double-knockout mice. All mice are in C57BL/6J background and were backcrossed for eight generations following the standard backcrossing procedure. Male mice were used and analyzed at 6–8 or 12 weeks. For control and experimental group, *Pax7-Cre*$^{ERT2/ERT2}$, *Vgll4*$^{f/f}$ mice or *Pax7-Cre*$^{ERT2/ERT2}$,*Vgll4*$^{f/f}$,*Yap*$^{f/f}$ mice were analyzed to avoid the strain variation. Mice in the experimental group were intraperitoneally injected with tamoxifen, which is dissolved in sunflower oil. Mice in the control group were from the same strain and

intraperitoneally injected with sunflower oil (vehicle, no tamoxifen). Genomic DNA was extracted from mice tissues by cell lysis buffer (50 mM PH 8.0 Tris–HCl, 100 mM EDTA, 1% SDS), 20 mg/ml Proteinase-K (P78893-100MG, ABCONE), 4 mg/ml RNAase-A (9001-99-4, Sigma), protein precipitate buffer (7.5 M NH4AC), and DNA hydration buffer (100 mM Tris–HCl, 1 mM PH8.8 EDTA). Mouse genotyping was performed by PCR. The following are primers for genotyping.

$Vgll4^{-/-}$ genotyping forward primer: 5′-TCCAGCTGAGCGCCGGT CGCTACCA-3′; $Vgll4^{-/-}$ genotyping reverse primer 1: 5′-GACCA CGTCTCCAAGATGAGCCGCA-3′; $Vgll4^{-/-}$ genotyping reverse primer 2: 5′-GCATAATGGCCAGCAGAGGAGACTG-3′; $Vgll4^{f/f}$ genotyping forward primer: 5′-TTCTTCTGGCCTCCATGGGCATTGT-3′; $Vgll4^{f/f}$ genotyping reverse primer: 5′-ATGTTATCAGCAGTCGGGCG GGAA-3′; $Yap^{f/f}$ genotyping forward primer: 5′-AAGGTACTCCCA GTGCAACTC-3′; $Yap^{f/f}$ genotyping reverse primer: 5′-ATGCAAAGG CCACACTGTTC-3′; $Pax7$-Cre^{ERT2} genotyping forward primer: 5′-GC TGCTGTTGATTACCTGGC-3′; $Pax7$-Cre^{ERT2} genotyping reverse primer1: 5′-CTGCACTGAGACAGGACCG-3′; $Pax7$-Cre^{ERT2} genotyping reverse primer2: 5′-CAAAAGACGGCAATATGGTG-3′.

Cell lines and cell culture

Human 293T cells (ATCC) and mouse C2C12 cells (ATCC) were cultured in growth medium consisting of DMEM (Gibco) supplemented with 4.5 g glucose, 10% fetal bovine serum, and 1% Penicillin/Streptomycin at 37°C in a 5% CO_2 atmosphere. Medium was changed to differentiation medium (DMEM) containing 2% horse serum and 1% Penicillin/Streptomycin to induce differentiation of C2C12 cells. Cells were maintained in differentiation medium for up to 72 h. MuSCs were maintained on collagen-coated dishes in Ham's F-10 Nutrient Mixture (Gibco) [20% FBS, 2.5 ng/ml bFGF (Invitrogen)], T-cell conditional medium (F10 medium with 20% FBS : T-cell medium = 50 : 50), or cytokine cocktail medium (F10 medium containing 20% FBS, 5 ng/ml IL-1α, 5 ng/ml IL-13, 10 ng/ml IFN-γ, 10 ng/ml TNF-α, and 2.5 ng/ml FGF; Fu *et al*, 2015). Cultures were routinely passaged as they reached 60–70% confluence. MuSCs were differentiated in differentiation medium (DMEM with 2% horse serum). All cells were regularly checked for mycoplasma contamination once a month using the Mycoplasma detection kit (Genecopoeia, CAT#MP001). Primers used for mycoplasma detection are listed as follows: forward primer: 5′-GGGAGCAAAC AGGATTAGATACCCT-3′; reverse primer: 5′-TGCACCATCTGTCA CTCTGTTAACCTC-3′.

CTX injury

Muscle injury was induced by the injection of CTX (Sigma-Aldrich) to TA muscles. Briefly, 10 μl of 10 μM CTX was injected at each injection site using 28 gauge needles. For TA muscles, five injections were performed for one piece of TA muscles of 6- to 8-week-old mice. To induce genetic deletion in MuSCs, mice were performed by intraperitoneal injection of 10 mg/ml tamoxifen in sunflower oil (0.05 mg per gram body mice) daily for 5 days prior to injury. *Pax7-cre^{ERT2/ERT2},Vgll4^{f/f}* or *Pax7-Cre^{ERT2/ERT2},Vgll4^{f/f},Yap^{f/f}* mice with intraperitoneal injection of sunflower oil were considered as vehicle control. TA muscles were collected and analyzed at day 3, day 5, and day 7 after CTX injury.

Immunostaining and microscopy

For each experiment, the TA muscles were derived from at least 4 mice. For each TA muscle, over 30 serial cryo-sections were excised, and the maximum cross-sectional area was picked out for immunostaining and quantification. For each MuSC population from one mouse, two different slides were made. For immunostaining of MuSCs, the same number of MuSCs isolated from different mice lines was seeded and performed exactly the same operations after seeding. For immunostaining of C2C12 myoblasts, the same number of cells from each group was seeded. TA muscles' frozen sections, single fiber from EDL muscles, MuSCs-derived myoblasts, or C2C12 myoblasts were fixed in 4% formaldehyde in PBS buffer at room temperature for 10 min, washed with PBS buffer, and then treated with PBST (PBS and 0.25% Triton X-100) for permeabilization. Cells or frozen sections were blocked with PBSA (PBS and 3% BSA) for 30 min and incubated with primary antibody overnight in PBSA at 4°C. Primary antibodies used in this study were as follows: rabbit anti-Laminin (1:500, abcam, ab11575), rat anti-Laminin (1:500, abcam, ab11576), rabbit anti-Desmin (1:500, abcam, ab15200), mouse anti-MyHC (1:1,000, Millipore, 05-716), and rabbit anti-GFP-488 (1:200, abcam, ab6662). Afterward, cells were washed with PBST and incubated with secondary antibody diluted in PBSA for 1 h at room temperature. Secondary antibodies used were Alexa Fluor 488, 552, or 647-conjugated goat anti-mouse, goat anti-rabbit, or goat anti-rat with a dilution of 1:1,000. DAPI was used to stain the nuclei. Samples were mounted with Aqua-Poly/Mount (Polysciences). Specially, Pax7 (1:200, DHSB, RRID:AB_528428) was stained as previously described (Fu *et al*, 2015). Immunofluorescent sections were imaged on Leica SP8 confocal microscope.

Fiber size distribution and fusion index

Cross-sectional area of the myofibers was calculated on section images obtained from TA muscles using Image J. MyHC staining was performed to define the outline of the myotubes, and cell containing three or more nuclei was considered as a myotube. To quantify the fusion of MuSCs and C2C12 cells, total cell nuclei and nuclei within myotubes were counted using Image J. Fusion index was calculated as the number of nuclei in myotubes divided by the total number of nuclei counted.

EdU incorporation

Seven-week-old mice were given intraperitoneal injection of EdU (Invitrogen, 0.05 mg per gram body weight) two consecutive days before analyzed. EdU was detected with the Click-iT EdU imaging kit (Invitrogen). About 200 nuclei per sample from one mouse were counted. EdU and Pax7 double-positive nuclei, EdU-positive nuclei, and total cell nuclei were counted using Image J.

Muscle functional assay

The male mice were analyzed at 12 weeks of age. Muscle function could be characterized by parameters such as maximum twitch force and maximum tetanic force by muscle test system 1200A/1300A from Aurora Scientific Asia. The protocols are supplied on Aurora Scientific Asia company web site. Three maximum isometric

twitch and tetanic forces were acquired using a train of 150 Hz in the muscles, and the highest number was recorded.

Muscle satellite cells isolation and FACS

MuSCs were isolated as previously described (Liu *et al*, 2015). Briefly, hindlimb muscles were dissected and carefully minced. Muscles were digested with collagenase II (800 units/ml) in washing medium (Ham's F10 with 10% horse serum) at 37°C for 90 min. Digested muscles were triturated and washed in washing medium before being subjected to further digestion with collagenase II (80 units/ ml) and dispase (1 unit/ml) for 30 min. The resulting suspensions were passed through a 20G needle attached to a syringe 15 times and filtered with a 40-mm cell strainer. Mononuclear cells were stained with antibodies Vcam1-biotin (BioLegend, 105704), CD11b-PerCP-Cy5.5 (BD Biosciences, 550993), CD31-PerCP-Cy5.5 (BD Biosciences, 562861), CD45-PerCP-Cy5.5 (BD Biosciences, 562861), and Sca1-Alexa Flour 647 (Thermo Fisher Scientific, MSCA2). The Vcam1 signal was amplified with streptavidin-PE-cy7. FACS analysis was performed, and cells with Sca1$^-$/CD11b$^-$/ CD31$^-$/CD45$^-$/VCAM1$^+$ signals represent the population of MuSCs. Differentiation was induced to confirm that the differentiation potential of MuSCs. All antibodies were used at a dilution of 1:75. The BD Influx cell sorter (BD Biosciences) was used for MuSCs sorting following the manufacturer's instructions.

Immunoblotting and immunoprecipitation

Immunoblotting and immunoprecipitation were performed as described previously (Wang *et al*, 2015). The protease inhibitor cocktail (HY-K0010) were purchased from MedChem Express. All the antibodies used in this study were commercial and had been validated. Antibodies used in this paper were as follows: mouse anti-FLAG (1:1,000, Sigma, F3165), mouse anti-MYC (1:1,000, Proteintech Group, 60003-2-Ig), mouse anti-HA (1:1,000, Sigma, H3663), mouse anti-His (1:1,000, Sigma, H1029), mouse anti-Lamin B1 (1:1,000, Abcam, ab16048), mouse anti-GAPDH (1:10,000, ABclonal, AC033), mouse anti-Tubulin (1:5,000, DSHB, E7), mouse anti-Histone H3 (1:5,000, Cell signaling, 9715), mouse anti-MyHC (1:1,000, upstate, 05-716), mouse anti-MyoG (1:1,000, Santa Cruz, sc-12732), mouse anti-MyoD (1:1,000, Santa Cruz, sc-32758), rabbit anti-VGLL4 (1:1,000, ABclonal, A18248), rabbit anti-TEAD1 (1:1,000, ABclonal, A6768), rabbit anti-TEAD2 (1:1,000, ABclonal, A15594), rabbit anti-TEAD3 (1:1,000, ABclonal, A7454), mouse anti-TEAD4 (1:1,000, Abcam, ab58310).

Real-time PCR

Total RNA was isolated using Trizol reagent (Invitrogen). Coding DNA was synthesized with ReverTra Ace qPCR RT master Mix with gDNA Remover kit (Invitrogen). RT–PCR was performed on ABI Fast 7500 using SYBR Green (Takara). The standard comparative CT quantization method ($\Delta\Delta C_t$) was used to analyze the RT–qPCR results (Livak & Schmittgen, 2001; Khan-Malek & Wang, 2011). The $\Delta\Delta C_t$ model is given by the formula Ratio = $2^{-\Delta\Delta Ct}$, where $\Delta\Delta Ct = \Delta Ct_{Treated} - \Delta Ct_{Control}$, $\Delta Ct_{Treated}$ is the C_t difference of a reference and target gene for a treated sample (i.e., $\Delta Ct_{Treated} = Ct_{Target} - Ct_{Ref}$), and $\Delta Ct_{Control}$ is the C_t difference of a reference and target

gene for a control sample (i.e., $\Delta Ct_{Control} = Ct_{Target} - Ct_{Ref}$). GAPDH was used as normalization control. For qPCR results that involve time course analysis, the values of time point 0 from control group were used for normalization. Primers for real-time PCR were obtained from BioSune Biotechnology Co., Ltd. (Shanghai, China). mVGLL4-qPCR-F (5′-ATGAACAACAATATCGGCGTTCT-3′); mVGLL4-qPCR-R (5′-GGGCTCCATGCTGAATTTCC-3′); mTEAD1-qPCR-F (5′-CTCCGCTTTCCTTGAACAGC-3′); mTEAD1-qPCR-R (5′-GTCCACAGATTCGAGCAACG-3′); mTEAD2-qPCR-F (5′-TGAGCAGCCAGTATGAGAGC-3′); mTEAD2-qPCR-R (5′-CAGCAGACGGTACACAAAGC-3′); mTEAD3-qPCR-F (5′-GATTGCCCGCTACATCAAGC-3′); mTEAD3-qPCR-R (5′-ATGCCAACCTGGTATTCCCG-3′); mTEAD4-qPCR-F (5′-AGCTAAGAACAAGGCCCTGC-3′); mTEAD4-qPCR-R (5′-TGCCAAAACCCTGAGATTGC-3′); mMyHC-qPCR-F (5′-CGCAGAATCGCAAGTCAATA-3′); mMyHC-qPCR-R (5′-ATATCTTCTGCCCTGCACCA-3′); mMyoG-qPCR-F (5′-CGGCTGCCTAAAGTGGAGAT-3′); mMyoG-qPCR-R (5′-AGGCCTGTAGGCGCTCAA-3′); mMCK-qPCR-F (5′-CACCTCCACAGCACAGACAG-3′); mMCK-qPCR-R (5′-ACCTTGGCCATGTGATTGTT-3′); mCYR61-qPCR-F (5′-AGAGGCTTCCTGTCTTTGGC-3′); mCYR61-qPCR-R (5′-CTCGTGTGGAGATGCCAGTT-3′); mCTGF-qPCR-F (5′-TCCGGACACCTAAAATCGCC-3′); mCTGF-qPCR-R (5′-TTCATGATCTCGCCATCGGG-3′); mGAPDH-qPCR-F (5′-CTCCCACTCTTCCACCTTCG-3′); mGAPDH-qPCR-R (5′-TAGGGCCTCTCTTGCTCAGT-3′).

ChIP assay

Cells were fixed with 1% formaldehyde for 10 min at room temperature. Nuclei were isolated and chromatins were extracted from the nuclei using ChIP sonication cell lysis buffer and nuclear lysis buffer (Cell signaling) with Protease Inhibitor Cocktail (HY-K0010, MedChem Express). The chromatins were then sheared to 200–500 bp by sonication (Qsonica). Antibodies against mouse IgG (Santa Cruz, sc-2025) and TEAD4 (Abcam, ab58310) were applied. The DNA immunoprecipitated by the antibodies was detected by RT–qPCR. The primers used are listed below: mMyoG-TBS-ChIP-qPCR-F (5′-TTGTTCCCTTCCTGCCCTGTCC-3′); mMyoG-TBS-ChIP-qPCR-R (5′-GGAGGCCGTCGGCTGTAATTTG-3′).

Plasmids construction

VGLL4, VGLL4-ΔTDU, VGLL4-HF4A, TEAD4, TEAD4-N, and TEAD4-C were constructed into pCDNA3.1(+)-FLAG/MYC and pLEX-HA lentiviral vectors. MyoG and MyoD were constructed into pCDNA3.1(+)-FLAG/MYC vector by the ClonExpress II One Step Cloning kit (Vazyme Biotech Co., Ltd, C112-02). To generate VGLL4 knockdown constructs, the following oligonucleotides were cloned into pLKO.1 vector at the AgeI/EcoRI sites: mVGLL4-shRNA-F:5′-CCGGGTTCTGTGCTATGAAGGTGAACTCGAG TTCACCTTCATAGCACAGAACTTTTTTG-3′; mVGLL4-shRNA-R:5′-AATTCAAAAAAGTTCTGTGCTATGAAGGTGA ACTCGAGTTCACCTTCATAGCACAGAACT-3′.

Notably, the VGLL4 shRNA targeting sequences are different from VGLL4 siRNA targeting sequences used in this study.

A scramble DNA duplex was also designed as control.
shLuciferase-F:5′-CCGGTTCCTGGAACAATTGCTTTTACTCGAGTAA
AAGCAATTGTTCCAGGAATTTTTG-3′;
shLuciferase-R:5′-AATTCAAAAATTCCTGGAACAATTGCTTTTACTC
GAGTAAAAGCAATTGTTCCAGGAA-3′.

Protein purification and GST pull-down assays

Mouse MyoD was cloned into pGEX-4T-1-GST vector and expressed in *E. coli* BL21 (DE3) cells. Human TEAD4-TEA and TEAD4-TEA-Q103A/V104R mutant were cloned into HT-pET-28a-HIS-SUMO vector and expressed in *E. coli* BL21 (DE3) cells. Glutathione agarose beads (GE) and Ni-NTA beads were used to purify the indicated proteins. HIS-SUMO coupled on Ni-NTA beads or GST-fused proteins coupled on Glutathione agarose beads (GE) were mixed with different prey proteins in pull-down lysis buffer (20 mM Tris–Cl pH 8.0, 200 mM NaCl, 1 mM EDTA, 0.5% NP-40, and 1% PMSF) at 4°C for 1 h, followed by washing three times with pull-down lysis buffer. The proteins bound on the Ni-NTA beads were eluted by the elution buffer (20 mM HEPES-KOH pH 7.5, 500 mM NaCl, 400 mM Imidazole, 20% Glycerin). The input and output samples were loaded to SDS–PAGE and detected by coomassie blue staining or Western blotting.

RNA interference

Mouse VGLL4 siRNA and mouse TEAD4 siRNA and the control siRNA were obtained from Shanghai GenePharma, Co., Ltd., Shanghai, China. siRNA oligonucleotides were transfected in C2C12 myoblasts by Lipofectamine RNAiMAX (Invitrogen) following the manufacturer's instructions. Two pairs of siRNAs were used to perform experiments. siRNAs used in this study are listed below:
siVGLL4-1: 5′-GACAAGATGAACAACAATATCTT-3′;
siVGLL4-2: 5′-ACACATGGCTTCAGATCAAAGTT-3′;
siTEAD4-1: 5′-ACTATTTGTACCGCATCCATT-3′;
siTEAD4-2: 5′-ATTTGTACCGCATCCACCGTT-3′.

siCtrl was used as the scramble control siRNA. The control siRNA sequence is: 5′-UUCUCCGAACGUGUCACGUTT-3′.

Transfection and viral infection

Transfection of plasmids was performed using Lipofectamine 3000 (Invitrogen) according to the manufacturer's instructions. To generate all sorts of stable cells, lentiviral infection was used. Briefly, HEK293T cells were co-transfected with viral vectors and packaging plasmids. 48 h after transfection, the progeny viruses released from HEK293T cells were filtered through a 0.45-μm filter and collected to infect cells of interest. 36–48 h after infection, cells were selected with 4 μg/ml puromycin in culture medium. The medium that contained puromycin was changed every 2–3 days.

Scanning electron microscope

Fresh EDL muscles were initially fixed with 2.5% glutaraldehyde at room temperature for 2 h and then at 4°C overnight. Muscles were washed in 0.1 M phosphate buffer by three times, 10 min at a time. The muscles were fixed in 1% osmic acid about 1 h and then were

washed in 0.1 M phosphate buffer once more. Tissues were dehydrated by the critical point drying method after ascending series of ethanol. The structures of EDL fibers were observed by scanning electron microscope after gold spraying.

MTT assay

The same number of cells was seeded in 96-well plate, and the viability of cells was measured by MTT assay daily for 5 days. Briefly, 20 μl of MTT working solution (5 mg/ml) was added into each well and incubated at 37°C for 4 h. Then, the supernatants were removed and the resultant MTT formazan was dissolved in 100 μl of DMSO. The absorbance was measured at the wavelengths of 595 and 630 nm.

Luciferase reporter assay

MyoG-TBS region was cloned into the pGL3-Basic vector and can be found in database NC_000067.6 (134289674-134289854). MyoG-(TBS+E) region was cloned into the pGL3-Basic vector and can be found in database NC_000067.6 (134289674-134290053). C2C12 cells were seeded in 24-well plates. The Gal4-TEAD4 construct was kindly given by professor Bin Zhao (Zhejiang University; Zhao *et al*, 2008). Luciferase reporter plasmid (0.5 μg) and the indicated plasmids (0.5 μg) were transfected to C2C12 cells. CMV-Renilla (0.005 μg) was transfected together to normalize the transfection efficiency. Luciferase activities were measured 48 h after transfection using Dual-Luciferase Assay kit (Promega) on GloMax 20/20 luminometer (Promega) following the manufacturer's instructions. Relative luciferase activity was calculated as the ratio of luciferase/Renilla activity. Experiments were done in triplicates.

Statistical analysis

Comparisons between groups were analyzed using an unpaired Student's *t*-test by GraphPad Prism. For data based on three samples, variants were compared by nonparametric test (Mann–Whitney unpaired test). Statistical parameters including the definitions and exact values of n, statistical test, and statistical significance were reported in the Figures and Figure Legends. Differences are statistically significant at $P < 0.05$. *$P < 0.05$; **$P < 0.01$; ***$P < 0.001$; ns, no significance. All data were presented as mean ± SEM. Every experiment was repeated independently. For each experiment, at least three biological replicates were processed.

Expanded View for this article is available online.

Author contributions

Conflict of interest

The authors declare that they have no conflict of interest.

References

Allen DL, Sartorius CA, Sycuro LK, Leinwand LA (2001) Different pathways regulate expression of the skeletal myosin heavy chain genes. *J Biol Chem* 276: 43524−43533

Anbanandam A, Albarado DC, Nguyen CT, Halder G, Gao X, Veeraraghavan S (2006) Insights into transcription enhancer factor 1 (TEF-1) activity from the solution structure of the TEA domain. *Proc Natl Acad Sci USA* 103: 17225−17230

Battistelli C, Busanello A, Maione R (2014) Functional interplay between MyoD and CTCF in regulating long-range chromatin interactions during differentiation. *J Cell Sci* 127: 3757−3767

Berkes CA, Bergstrom DA, Penn BH, Seaver KJ, Knoepfler PS, Tapscott SJ (2004) Pbx marks genes for activation by MyoD indicating a role for a homeodomain protein in establishing myogenic potential. *Mol Cell* 14: 465−477

Berkes CA, Tapscott SJ (2005) MyoD and the transcriptional control of myogenesis. *Semin Cell Dev Biol* 16: 585−595

Blackwell TK, Weintraub H (1990) Differences and similarities in DNA-binding preferences of MyoD and E2A protein complexes revealed by binding site selection. *Science* 250: 1104−1110

Brack AS, Rando TA (2012) Tissue-specific stem cells: lessons from the skeletal muscle satellite cell. *Cell Stem Cell* 10: 504−514

Buckingham M, Rigby PW (2014) Gene regulatory networks and transcriptional mechanisms that control myogenesis. *Dev Cell* 28: 225−238

Chen HH, Mullett SJ, Stewart AF (2004) Vgl-4, a novel member of the vestigial-like family of transcription cofactors, regulates alpha1-adrenergic activation of gene expression in cardiac myocytes. *J Biol Chem* 279: 30800−30806

Comai G, Tajbakhsh S (2014) Molecular and cellular regulation of skeletal myogenesis. *Curr Top Dev Biol* 110: 1−73

Davidson I, Xiao JH, Rosales R, Staub A, Chambon P (1988) The HeLa cell protein TEF-1 binds specifically and cooperatively to two SV40 enhancer motifs of unrelated sequence. *Cell* 54: 931−942

Dong J, Feldmann G, Huang J, Wu S, Zhang N, Comerford SA, Gayyed MF, Anders RA, Maitra A, Pan D (2007) Elucidation of a universal size-control mechanism in *Drosophila* and mammals. *Cell* 130: 1120−1133

Fu X, Xiao J, Wei Y, Li S, Liu Y, Yin J, Sun K, Sun H, Wang H, Zhang Z *et al* (2015) Combination of inflammation-related cytokines promotes long-term muscle stem cell expansion. *Cell Res* 25: 655−673

Guo T, Lu Y, Li P, Yin MX, Lv D, Zhang W, Wang H, Zhou Z, Ji H, Zhao Y *et al* (2013) A novel partner of Scalloped regulates Hippo signaling via antagonizing Scalloped-Yorkie activity. *Cell Res* 23: 1201−1214

Harvey KF, Zhang X, Thomas DM (2013) The Hippo pathway and human cancer. *Nat Rev Cancer* 13: 246−257

Hasty P, Bradley A, Morris JH, Edmondson DG, Venuti JM, Olson EN, Klein WH (1993) Muscle deficiency and neonatal death in mice with a targeted mutation in the myogenin gene. *Nature* 364: 501−506

Hayashi S, Tenzen T, McMahon AP (2003) Maternal inheritance of Cre activity in a Sox2Cre deleter strain. *Genesis* 37: 51−53

Heidt AB, Rojas A, Harris IS, Black BL (2007) Determinants of myogenic specificity within MyoD are required for noncanonical E box binding. *Mol Cell Biol* 27: 5910−5920

Jiao S, Wang H, Shi Z, Dong A, Zhang W, Song X, He F, Wang Y, Zhang Z, Wang W *et al* (2014) A peptide mimicking VGLL4 function acts as a YAP antagonist therapy against gastric cancer. *Cancer Cell* 25: 166−180

Jiao S, Li C, Hao Q, Miao H, Zhang L, Li L, Zhou Z (2017) VGLL4 targets a TCF4-TEAD4 complex to coregulate Wnt and Hippo signalling in colorectal cancer. *Nat Commun* 8: 14058

Joshi S, Davidson G, Le Gras S, Watanabe S, Braun T, Mengus G, Davidson I (2017) TEAD transcription factors are required for normal primary myoblast differentiation *in vitro* and muscle regeneration *in vivo*. *PLoS Genet* 13: e1006600

Judson RN, Tremblay AM, Knopp P, White RB, Urcia R, De Bari C, Zammit PS, Camargo FD, Wackerhage H (2012) The Hippo pathway member Yap plays a key role in influencing fate decisions in muscle satellite cells. *J Cell Sci* 125: 6009−6019

Khan-Malek R, Wang Y (2011) Statistical analysis of quantitative RT-PCR results. *Methods Mol Biol* 691: 227−241

Kim CH, Neiswender H, Baik EJ, Xiong WC, Mei L (2008) Beta-catenin interacts with MyoD and regulates its transcription activity. *Mol Cell Biol* 28: 2941−2951

Kokabu S, Nakatomi C, Matsubara T, Ono Y, Addison WN, Lowery JW, Urata M, Hudnall AM, Hitomi S, Nakatomi M *et al* (2017) The transcriptional co-repressor TLE3 regulates myogenic differentiation by repressing the activity of the MyoD transcription factor. *J Biol Chem* 292: 12885−12894

Koontz LM, Liu-Chittenden Y, Yin F, Zheng Y, Yu J, Huang B, Chen Q, Wu S, Pan D (2013) The Hippo effector Yorkie controls normal tissue growth by antagonizing scalloped-mediated default repression. *Dev Cell* 25: 388−401

Liu L, Cheung TH, Charville GW, Rando TA (2015) Isolation of skeletal muscle stem cells by fluorescence-activated cell sorting. *Nat Protoc* 10: 1612−1624

Livak KJ, Schmittgen TD (2001) Analysis of relative gene expression data using real-time quantitative PCR and the 2(-Delta Delta C(T)) method. *Methods* 25: 402−408

Maeda T, Chapman DL, Stewart AF (2002) Mammalian vestigial-like 2, a cofactor of TEF-1 and MEF2 transcription factors that promotes skeletal muscle differentiation. *J Biol Chem* 277: 48889−48898

Mal A, Sturniolo M, Schiltz RL, Ghosh MK, Harter ML (2001) A role for histone deacetylase HDAC1 in modulating the transcriptional activity of MyoD: inhibition of the myogenic program. *EMBO J* 20: 1739−1753

Mal AK (2006) Histone methyltransferase Suv39h1 represses MyoD-stimulated myogenic differentiation. *EMBO J* 25: 3323−3334

Murphy MM, Lawson JA, Mathew SJ, Hutcheson DA, Kardon G (2011) Satellite cells, connective tissue fibroblasts and their interactions are crucial for muscle regeneration. *Development* 138: 3625−3637

Nabeshima Y, Hanaoka K, Hayasaka M, Esumi E, Li S, Nonaka I, Nabeshima Y (1993) Myogenin gene disruption results in perinatal lethality because of severe muscle defect. *Nature* 364: 532−535

Pan D (2010) The hippo signaling pathway in development and cancer. *Dev Cell* 19: 491−505

Paulmurugan R, Umezawa Y, Gambhir SS (2002) Noninvasive imaging of protein-protein interactions in living subjects by using reporter protein complementation and reconstitution strategies. *Proc Natl Acad Sci USA* 99: 15608−15613

Peng XL, So KK, He L, Zhao Y, Zhou J, Li Y, Yao M, Xu B, Zhang S, Yao H *et al* (2017) MyoD- and FoxO3-mediated hotspot interaction orchestrates super-enhancer activity during myogenic differentiation. *Nucleic Acids Res* 45: 8785−8805

Pobbati AV, Hong W (2013) Emerging roles of TEAD transcription factors and its coactivators in cancers. *Cancer Biol Ther* 14: 390−398

Polesskaya A, Harel-Bellan A (2001) Acetylation of MyoD by p300 requires more than its histone acetyltransferase domain. *J Biol Chem* 276: 44502−44503

Polesskaya A, Naguibneva I, Duquet A, Bengal E, Robin P, Harel-Bellan A (2001) Interaction between acetylated MyoD and the bromodomain of CBP and/or p300. *Mol Cell Biol* 21: 5312−5320

Reynaud EG, Leibovitch MP, Tintignac LA, Pelpel K, Guillier M, Leibovitch SA (2000) Stabilization of MyoD by direct binding to p57(Kip2). *J Biol Chem* 275: 18767−18776

Seale P, Rudnicki MA (2000) A new look at the origin, function, and "stem-cell" status of muscle satellite cells. *Dev Biol* 218: 115−124

Shi Z, He F, Chen M, Hua L, Wang W, Jiao S, Zhou Z (2017) DNA-binding mechanism of the Hippo pathway transcription factor TEAD4. *Oncogene* 36: 4362−4369

Shirakata M, Paterson BM (1995) The E12 inhibitory domain prevents homodimer formation and facilitates selective heterodimerization with the MyoD family of gene regulatory factors. *EMBO J* 14: 1766−1772

Skarnes WC, Rosen B, West AP, Koutsourakis M, Bushell W, Iyer V, Mujica AO, Thomas M, Harrow J, Cox T *et al* (2011) A conditional knockout resource for the genome-wide study of mouse gene function. *Nature* 474: 337−342

Stewart AF, Suzow J, Kubota T, Ueyama T, Chen HH (1998) Transcription factor RTEF-1 mediates alpha1-adrenergic reactivation of the fetal gene program in cardiac myocytes. *Circ Res* 83: 43−49

Tajonar A, Maehr R, Hu G, Sneddon JB, Rivera-Feliciano J, Cohen DE, Elledge SJ, Melton DA (2013) Brief report: VGLL4 is a novel regulator of survival in human embryonic stem cells. *Stem Cells* 31: 2833−2841

Tapscott SJ (2005) The circuitry of a master switch: Myod and the regulation of skeletal muscle gene transcription. *Development* 132: 2685−2695

Wang C, Zhang W, Yin MX, Hu L, Li P, Xu J, Huang H, Wang S, Lu Y, Wu W *et al* (2015) Suppressor of Deltex mediates Pez degradation and modulates *Drosophila* midgut homeostasis. *Nat Commun* 6: 6607

Weintraub H, Tapscott SJ, Davis RL, Thayer MJ, Adam MA, Lassar AB, Miller AD (1989) Activation of muscle-specific genes in pigment, nerve, fat, liver, and fibroblast cell lines by forced expression of MyoD. *Proc Natl Acad Sci USA* 86: 5434−5438

Weintraub H, Dwarki VJ, Verma I, Davis R, Hollenberg S, Snider L, Lassar A, Tapscott SJ (1991) Muscle-specific transcriptional activation by MyoD. *Genes Dev* 5: 1377−1386

Yin H, Price F, Rudnicki MA (2013) Satellite cells and the muscle stem cell niche. *Physiol Rev* 93: 23−67

Yu FX, Zhao B, Guan KL (2015) Hippo pathway in organ size control, tissue homeostasis, and cancer. *Cell* 163: 811−828

Yu W, Ma X, Xu J, Heumuller AW, Fei Z, Feng X, Wang X, Liu K, Li J, Cui G *et al* (2019) VGLL4 plays a critical role in heart valve development and homeostasis. *PLoS Genet* 15: e1007977

Yuan W, Condorelli G, Caruso M, Felsani A, Giordano A (1996) Human p300 protein is a coactivator for the transcription factor MyoD. *J Biol Chem* 271: 9009−9013

Yun K, Wold B (1996) Skeletal muscle determination and differentiation: story of a core regulatory network and its context. *Curr Opin Cell Biol* 8: 877−889

Zhang L, Ren F, Zhang Q, Chen Y, Wang B, Jiang J (2008) The TEAD/TEF family of transcription factor Scalloped mediates Hippo signaling in organ size control. *Dev Cell* 14: 377−387

Zhang W, Gao Y, Li P, Shi Z, Guo T, Li F, Han X, Feng Y, Zheng C, Wang Z *et al* (2014) VGLL4 functions as a new tumor suppressor in lung cancer by negatively regulating the YAP-TEAD transcriptional complex. *Cell Res* 24: 331−343

Zhao B, Wei X, Li W, Udan RS, Yang Q, Kim J, Xie J, Ikenoue T, Yu J, Li L *et al* (2007) Inactivation of YAP oncoprotein by the Hippo pathway is involved in cell contact inhibition and tissue growth control. *Genes Dev* 21: 2747−2761

Zhao B, Ye X, Yu J, Li L, Li W, Li S, Yu J, Lin JD, Wang CY, Chinnaiyan AM *et al* (2008) TEAD mediates YAP-dependent gene induction and growth control. *Genes Dev* 22: 1962−1971

Zhao B, Tumaneng K, Guan KL (2011) The Hippo pathway in organ size control, tissue regeneration and stem cell self-renewal. *Nat Cell Biol* 13: 877−883